CHARACTERIZATION AND MODELING THE DISSOLUTION PERFORMANCE OF TABLETS FOCUSING ON POWDER PROCESSING EFFECTS

BY DANIEL BRAIDO

A dissertation submitted to the

Graduate School—New Brunswick

Rutgers, The State University of New Jersey

in partial fulfillment of the requirements

for the degree of

Doctor of Philosophy

Graduate Program in Chemical and Biochemical Engineering

Written under the direction of

Professor Alberto Cuitino

and approved by

_____

_____

_____

_____

New Brunswick, New Jersey

October, 2012

ABSTRACT OF THE DISSERTATION

Characterization and Modeling the Dissolution Performance of Tablets Focusing on Powder Processing Effects

by Daniel Braido

Dissertation Director: Professor Alberto Cuitino

Tablet dissolution modeling has seen many efforts from both empirical and physical approaches. We present an expandable 3-D Cartesian framework for modeling multiple physical processes involved in tablet dissolution, which allows for a more straightforward generation of models while maintaining powerful model manipulation. Also presented is an experimental technique for quantifying solvent penetration and dynamic surface erosion. Two types of solid oral dosage forms are experimentally characterized and then modeled. One system is governed by drug particle dissolution, the other by surface erosion.

Acknowledgements

I am grateful to Professor Alberto Cuitino for being patient with my progress, and helping to put me back on the right track when my course became too tangential to the work. His support was instrumental in my success. I would also like to thank Professor Fernando Muzzio for giving me the motivation to complete my work when the future was beginning to look bleak. I would like to thank Professor Bozena Michniak-Kohn for the regular input and feedback concerning the dissolution experiments as well as access to the necessary experimental equipment. In addition, I would like to thank all three as well as Professor Rohit Ramachandran for being a part of my defense committee. Dr. Kalyan Pingali, Dr. Marcos Llusa, and Dr. Rafael Mendez have also been instrumental in the development of the physical experiments and providing the background work for which this thesis is based. Dr. Athanas Koynov has provided me with great help both in the work entailed here and basic guidance in career path and life. Dr. Yuriy Gulak has also been instrumental in creating several experimental assays used herein and providing me with a great deal of otherwise hidden literature references. Golshid Keyvan has been extremely helpful in performing numerous dissolution assays over the past several years. I would also like to thank the undergraduate students who have been a part of this work; Gennadios Cassotis, Jeffrey Johnson, Rizwan Aslam, Nicole Sermabeikian, Joseph Hyman, Wanze Li, and Alfred Irungu. Included in the work herein are portions of research articles in or pending publication:

D Braido, Y Gulak and A M Cuitino, Solvent penetration rate in tablet measurement using video image processing., AAPS PharmSciTech 13(2):507-12 (2012) PMID 22426793

D Braido, A Dubey, F J Muzzio, A M Cuitino, Analysis of tablet content uniformity using Laser Induced Breakdown Spectroscopy., AIChE Journal, In Review

D Braido, A Koynov, A M Cuitino, A Modeling and Simulation Framework for Predicting Drug Release Concurrently Incorporating the Effects of Dissolution and Diffusion., Int. Journal of Pharmaceutics, Awaiting approval for submission

D Braido, F Romanski, W Li, A Cuitino, B Michniak-Kohn, Effect of Particle Size on Bioaccessibility of Griseofulvin Suspensions. In preparation

Dedication

I dedicate this thesis to my parents Louis and Susan Braido, and my wife Qin Braido and my son Ethan. Nothing would be possible without their continued support.

Table of Contents

Chapter 1

Introduction

Tablets are the most popular drug delivery dosage form currently in use due to their precision of dosage, mechanical and chemical stability and ease of storage and distribution, not to mention that they are also the most cost effective for mass production. A typical pharmaceutical tablet consists of several different powders, (such as actives, excipients, lubricants, glidants, disintegrants, etc.) compressed into a solid body. Usually administered orally, tablets disintegrate and dissolve in the gastro-intestinal tract, allowing for the active pharmaceutical ingredient(API) to be absorbed through the intestinal wall and into the blood stream where it is subsequently transported throughout the body[1]. While there are many physiological factors specific to the patient ingesting the dosage form, pharmaceutical manufacturers have no control over the unique biological processes of a specific patient. What can and should be controlled by the manufacturer are the formulation and processing conditions of the tablet which influence its in-vitro dissolution performance.

Pharmaceutical blends are often doped with small quantities of lubricants and glidants to improve flowability and compactibility[2]. The influence of formulation components on the drug release performance of tablets has been reported extensively in the literature. Specifically, interest has been paid to the volumetric content of lubricants, disintegrants, binders and API[3]. There has also been some work detailing the effects of magnesium stearate(MgSt) distribution on tablet performance as a result of over-blending.[4, 5, 6, 7, 8] A recent publication has shown that the smearing of flowing agents during the mixing process can cause variations in surface coatings of API and excipients altering the surface properties of powder particles in a pharmaceutical blend[7]. Emphasis was placed on the changes in surface coating properties due to the

mixing order of flowing agents, MgSt and colloidal silica(CS) and their influence on the final product in-vitro drug release. What is missing is an understanding of the precise mechanisms which effect these changes in product performance.

While there is no single type of pharmaceutical tablet, most can be considered as porous, heterogeneous solids, which when ingested, release drug product from their excipient matrices as a function of both their structure and the properties of the surrounding environment. It is this process of dissolution which product designers often strive to control, whether this means releasing all drug content as quickly as possible or in a controlled manner. In response to this need to understand how solid dosage forms will behave and isolate the governing mechanisms, multiple modeling methodologies have been developed and researched over the years[9]. The Noyes-Whitney equation[10] is considered to be the first published model dealing with dissolution of a solid and as such is referenced in most works regarding the subject. This work highlights the importance of the surface area of the dissolving solid in contact with solvent on the dissolution rate. This equation provided a basis for other works over the years including the Brunner equation [11]which accounts for dissolution rate dependence on the solid area available for dissolution and the the Hixson Crowell equation [12, 13] which adjusts the proportionality of the release rate to the amount of drug remaining in the solid (accounting for diminishing tablet dimensions). An alternative modeling route resulted in the development of the Higuchi equation [14, 15] (modified by Cobby[16] to apply to cylindrical tablets) which models the dissolution of drug particles dispersed in a uniform, homogeneous matrix. The model was augmented by Seki ([17]) to handle non-homogeneous matrices. The models attempted to incorporate the complexities of tablet microstructure and include the location of individual active particles inside the solid form. They account for tablet porosity, volume accessible to the dissolution media and an effective diffusion coefficient through the pore channels, but in an empirical manner. Slightly more recent progression in model development has yielded simulation tools accounting for tablet structure and geometric characteristics in the penetration of fluids - the Korsmeyer-Peppas model [18], as well as surface erosion (handled as a kinetic process) - the Hopfenberger model [19].

However, most current formulation design targeted at preset release profiles consists in large parts of trial and error with feed-back provided by large amounts of dissolution testing. This is often the case because the exact mechanisms controlling dissolution are not explicitly resolved, but the models are fit to experimental data after the fact. In an attempt to ameliorate the state of the art, over the last several years, the U.S. Food and Drug Administration(FDA) has championed the Process Analytical Technologies(PAT) and Quality by Design(QbD) initiatives. Aiming to provide a novel systematic approach for the design, analysis and control of manufacturing processes, QbD requires an in-depth, model-based understanding of the engineering and scientific principles involved and the identification of the variables, which affect product quality. After setting the targeted product profile Critical Quality Attributes(CQA) need to be identified. These are the product qualities affecting its performance as a time-controlled drug delivery device. The set of material characteristics and independent process parameters capable of affecting the CQAs is usually referred to as the set of critical process parameters. Determination of the range of each CPP that produces acceptable product allows for the establishment of a process design space. While experimental methods, such as dissolution testing can still serve an important role as a control mechanism, product quality cannot be tested in - it needs to be designed along with the product, on the foundation of physics and engineering-based models of the system. The last decade has seen tremendous progress in the implementation of numerical models for the study of pharmaceutical tablet dissolution. Current dissolution models have attained high levels of sophistication, simulating the change in diffusivity caused by the gradual penetration of the solvent into the tablet and the subsequent swelling of the polymer matrix [20]. The phenomena considered also include, active dissolution and the changes in porosity it produces as well as tablet surface erosion [21, 22].

In the following sections we describe a general level set based framework for simulating release profiles driven by erosion, dissolution and diffusion. This framework provides the basis for determining the boundary conditions of a set of partial differential equations which govern intra matrix transport. Our goal is not to redefine the physical processes

or numerical models governing dissolution, but to provide a basic frame work which can be easily modified to model multiple systems where more precise than grid resolution tracking of the solid liquid interface is desired. The individual mechanisms governing dissolution used herein can be modified or replaced as the system being considered is changed. The utilized mechanisms governing internal dissolution are similar to those used in other recent works concerning mechanistic dissolution models of tablets[22], however, their model considers the tablet fluid interface to exist at cell boundaries. The framework described here achieves spatial resolution of the boundaries at higher than grid resolution through the use of a level set based method. It is not the goal of this work to create an inherently new model of tablet dissolution, but to showcase the capabilities of this general technique in handling complex topological changes and incorporating multiple physical processes. The detailed generation of the model is followed by the creation and characterization of two rather different solid oral dosage systems. The first system is produced via a direct compression technique and explores the effect of different blending parameters on the resultant tablet properties, including the dissolution dominated drug release. The second system is created using a high shear wet granulation method prior to compaction, and drug release is erosion dominated. Both systems are characterized using a specifically tailored set of physical experiments, the results of which are used to describe their representations in the aforementioned in-silico model.

Chapter 2

Background

The purpose of this research is to investigate changes in the mechanisms governing tablet performance as a result of changes in formulation and processing conditions. Efforts will be made to characterize changes in the microstructure of different solid dosage forms and correlate these changes to the material properties of the different ingredients in the composite systems. As such, basic literature review concerning the numerical systems implemented, the physical systems being investigated and a technical explanation of the methodologies utilized in this research is presented herein. This includes discussions on prior efforts to model drug dissolution numerically, effects of blend processing on tablet performance, Laser Induced breakdown Spectroscopy(LIBS), X-ray μCT and solvent uptake.

2.1 Dissolution Modeling

The last several decades have seen tremendous progress in the implementation of numerical models for the study of pharmaceutical tablet dissolution. Of these, the simplest ones are based on zero-order kinetics, approximating a slow release system with no disagregation, which never reaches equilibrium conditions [23]. As the need to consider additional phenomena became apparent, first-order kinetics models were devised, taking into account the effects of the concentration of the dissolved drug in a diffusion layer around the tablet is the progenitor of tablet dissolution modeling - the Noyes-Whitney equation [10]; dissolution rate dependence on the solid area available for dissolution and the concentration already in solution - the Brunner equation [11]; the proportionality of the release rate relates to the amount of drug remaining in the solid (accounting for diminishing tablet dimensions) - the Hixson Crowell equation [12, 13]. Further insight

into the importance of tablet microstructure lead to the inclusion of the location of individual active particles inside the solid form. The Higuchi equation [14, 15] (modified by Cobby to apply to cylindrical tablets) models the dissolution of drug particles dispersed in a uniform, homogeneous matrix. It accounts for tablet porosity, volume accessible to the dissolution media and an effective diffusion coefficient through the pore channels. The model was augmented by Seki [17] to handle non-homogeneous matrices. Progression in model development has recently yielded simulation tools accounting for tablet structure and geometric characteristics - the Korsmeyer-Peppas model [18], as well as surface erosion (handled as a kinetic process) - the Hopfenberger model [19]. While these models strive to achieve detailed descriptions fo the physical systems, published results utilizing them consist primarily 1 and 2 dimensional efforts. Current dissolution models have attained high levels of sophistication, simulating the change in diffusivity caused by the gradual penetration of the solvent into the tablet and the subsequent swelling of the polymer matrix [20]. The phenomena considered also include, active dissolution and the changes in porosity it produces as well as tablet surface erosion [21]. Another approach is through the use of empirical models which seek to create basic decision engines from data already acquired from past physical experiments[24]. Multi-physics models which seek to model each of the processes individually, and coupling their results have also emerged.

Chief among these are the efforts of Stepanek et al. This group has recently published several models which focus on mesoscale tablet behavior. The most recent efforts stem from a model which represents portions of the tablet volume as "voxels"[22]. The tablet is modeled via a collection of cells each with their own given set of rules, similar to cellular automata. Results of 2-D simulations are compared to dynamic infrared images results of the top axial surface of a physical tablet undergoing dissolution. The bulk interface is defined to exist wherever there is an otherwise empty voxel, thus the boundary conditions are applied on a cell by cell basis, and assume bulk boundaries exist at cell boundaries. This means that diffusion of solute happens at particle boundaries, and there is no accountign for the diffusion of solute through a porous matrix or convection to the bulk solution at the tablet fluid interface. The scientists report good agreement

of the numerical results with analytical solutions of the model system. The model was adapted to use a discrete element approach[25, 26]. To achieve 3-D representation, particles were represented via hexagonal cylinders. This is not a true 3-D representation though, as in the case of physical tablets the distribution of active at the surface does not track directly along the central axis. This technique does however incorporate dynamic swelling. As each of the particles in the tablet is individually represented, its size can be directly computed as well as the effect on the location of surrounding particles. While the exact number of particles used in the simulation is not directly claimed, a basic analysis of the parametric space involved shows it is approximately 1000 particles. The authors claim this explicit definition of the component distribution as a key advantage[26]. This is a small number of particles in relation to what would exist in an average commercial pharmaceutical tablet. Furthermore, application of this model to a specific formulation system resulted in a model with 3 free parameters to match the physical results[25]. The numerical results align very well with results from physical experiments with compacts. This model could benefit greatly from extension to 3-D as this should increase the predictive power when evaluation commercial dosage forms.

2.2 Processing Effects

Glidants, lubricants and other anti-sticking agents such as Cab-O-Sil (CS) and magnesium stearate(MgSt) have been used in pharmaceutical powder blends in order to enhance their flowability [27, 28]. The concentrations of these excipients are critical to developing blends with improved flow, reduced die friction and improved tabletability. Addition of 0.5% by mass(sometimes even less) of colloidal silica to powder mixtures has been shown to improve their flowability[29]. Increasing the concentration of MgSt in powder blends has also been shown to improve tabletability, but also decreases dissolution rate[30]. Pharmaceutical blends are often complex mixtures and contain multiple flowing/lubricating agents, the effects of which can have interactions[31]. Pingali, et al. have shown that these excipients can have a compendious effect which is modulated by the shear processing history of these blends[7]. This interaction and modulation effect

applies not only to powder properties such as flowability, content uniformity and compressibility, but influences the resulting microstructure and subsequent performance of the tablets made from them. Shear histories of a blend are dependent on both scale and equipment and are thus subject to process changes which are a frequent reality of commercial manufacturing.

The mechanical strength of tablets has been shown to be affected by their excipient matrices[32, 33, 34], and there is work relating density and hardness to dissolution performance of tablets[30]. The previous findings show that when only MgSt was used in the formulation, the percentage of MgSt did not necessarily result in a change in the release rate or the total amount of drug released[34]. And while sometimes crushing strength was found to increase with increasing MgSt concentrations(0.22%),increasing mixing times of MgSt is known to decrease tablet hardness[35].

Several studies have been performed which investigate lubricant sensitivity,interactive mixtures and order of mixing in relation to tablet bonding properties[36, 37, 38, 24], but a mechanistic model describing tablet performance as a result of these formulation and processing conditions has not.

2.3 LIBS

Atomic emission spectroscopy of laser-produced plasma forms the basis of LIBS. In this technique, a laser pulse is focused on the surface of the sample to ablate a small amount of material resulting in the ionization of its constituent atoms. An optical spectrometer resolves the spectrum composed of atomic lines and molecular bands. The constituent elements of the ablated sample can thus be identified by analyzing the spectrum at wavelengths at which they emit light when decaying from high energy levels. A univariate calibration curve can be constructed to define the relationship between the emission intensity and the concentration of the species of interest. This leads to a simple and efficient way to quantify a formulation composition. PharmaLIBS250, an instrument manufactured by Pharmalaser Inc. was used in this study. It is divided into two compartments - the ablation chamber on the top is used to house the sample tray and laser

guide. The bottom part contains a computer and a spectrometer among other components. Neodymium-doped yttrium aluminum garnet (Nd:Y3Al5O12) or Nd:YAG Laser at 1064nm wavelength is passed through a beam sampler and a lens before it is redirected using a mirror on to the sample which is fixed in a placeholder on the carrousel. The light signal from the plasma is transmitted through a fiber optic bundle to the spectrometer and the CCD detector . Laser-Induced Breakdown Spectroscopy (LIBS) technology has been used to analyze materials in multiple fields including; metallurgy, environmental science, art conservation and planetary exploration[39, 40]. Within the past 10 years, LIBS use to analyze pharmaceutical products[41, 42, 43] has become prevalent in the literature. The LIBS technique, like other current chemical imaging techniques, has both strengths and limitations. Its comparably rapid speed of analysis, preparation free sampling, and avoidance of wet chemistry make it an increasingly useful option for in situ, real time qualitative analysis[44, 45, 46]. The situation is different for quantitative analysis. The variability in environmental and heterogeneous matrix properties make quantitative analysis with this technique more challenging. Even when environmental conditions are well controlled, signal measurements are influenced by the microstructural properties of the solid material being analyzed. For more precise quantitative analysis of elemental composition, LIBS requires standards, calibration curves, time and cost. In addition, consistent, high fidelity reconstructions of solid dosage forms is not feasible in most cases and impractical to repeat for samples to be analyzed. The LIBS technique involves ablation(influenced by the material and structure of the sample as well as working distance from the laser pulse focal point[44]), the production of free electrons, the absorption of the laser pulse by the plasma and the resulting plasma temperature. Multiple works have included analyses of the material being removed from samples with each pulse[47, 44, 48], but these results are often for metals instead of tablets made of organic materials. The Calibration-Free Laser-Induced Breakdown Spectroscopy (CF-LIBS) approach[49] has been reviewed from previous work, highlighting insights of multiple aspects of LIBS analysis. The experimental results shown herein are for an analysis of material ablation as a function of processing conditions. First, blends containing the same materials are blended then processed at different intensities

for different amounts of time. Tablets made from these blends are analyzed using a commercially available LIBS unit and the results analyzed to show trends in measurement changes associated with processing parameters. Certain processed batches were then subjected to a depth test where tablets were exposed to a different number of laser pulses at different locations and then shot depth was analyzed using X-ray μCT.

2.4 Solvent Penetration

The solvent/water penetration rate into the tablet often correlates well with the disintegration rate [50]. A swelling gel layer, formed during the penetration and acting as a diffusion barrier for active ingredients, may also affect their dissolution rate. Therefore, experimental measurements of the velocity of the liquid front are needed in order to adjust or optimize the drug performance. In addition, such measurements can help us understand the diffusion mechanism for a particular solvent - tablet matrix combination. It is observed that the mass transport through the polymer matrix often deviates from the Fickian diffusion theory, which predicts that the solvent front should advance as a square root of time. In contrast, a Case II mechanism, characterized by a sharp front moving linearly with time and practically uniform solvent concentration behind the front, is observed [51, 52]. The transitional non-Fickian behavior, called anomalous diffusion, is also possible, but can be hard to observe [53]. A number of experimental techniques have been developed for diffusion studies in polymers [54], consisting of two basic types of investigation: the diffusion front rates and the concentration profiles measurements. Clearly, time dependent solvent concentration profiles can provide more complete information about the diffusion mechanism, but are difficult to obtain and require quite sophisticated and expensive techniques such as nuclear magnetic resonance imaging, light and electron microscopy, Raman spectroscopy, and other methods described in [54]. Since the penetrating front is usually sharp, a wider choice of interface tracking methods is available that allows one to avoid the detailed concentration field measurements. One such technique, the ultrasound method [55], offers the possibility of continuous measurement of both the swelling and eroding fronts. A majority of the existing methods, however, require expensive equipment, special tablet samples

preparation, and time consuming data collection and processing. In the present work, we describe a simple technique of practical nature for solvent diffusion front tracking by visualizing the penetration process using digital video image processing. The goal is not a comprehensive study of a particular sample, but rather a fast diffusion rate estimation and comparison in multiple tablets of different formulations or process parameters. This technique is especially suitable for immediate release tablets that show relatively fast solvent penetration rate. It works well with commonly prepared tablets (i.e. compressed using a rotary tablet press), and does not necessarily require special samples preparation. Most of our results show close to linear penetration front advance that correspond to the non-Fickian or Case II sorption. It should be noted, that in some studies, the sorption ability of tablets is determined by measuring the absorbed mass with time using standard tensiometers [56]. Then, a velocity constant is obtained by fitting the experimental data to the Washburn-like equation [57] Morrissey and Vesely [58] argue, however, that the measurements of mass uptake are less valuable, since they cannot differentiate between the concentration level and the penetration distance. In addition, the question of applicability of the Washburn model to the case of non-Fickian sorption requires special attention and will be discussed below. There are several theories/models of the non-Fickian diffusion that can be used to interpret/fit the experimental penetration data (for recent overviews see [54, 59]). One such theory, developed by Thomas and Windle [60], recognizes that the kinematics of the penetration is controlled by the rate at which the polymer structure rearranges, or relaxes due to the solvent moving in. Wu and Peppas [61] extended the Thomas and Windle model by introducing a coupling between mass transport, driven by the concentration gradient and deformation in the polymer, based on the continuum mechanics formulation. They employed the Maxwell viscoelastic stress-strain constitutive relations so that a polymer relaxation time could be naturally defined. This model can describe a transition from Fickian to Case II transport depending on which process - solvent diffusion in a swollen polymer region or stress relaxation in the glassy region - advances at a slower rate. It is mathematically formulated as a boundary value problem for a system of coupled partial differential equations (PDEs) from which the time evolution

of the concentration and stress fields can be obtained numerically [62]. However, while the Wu-Peppas and similar models capture well physical mechanisms of the penetration and are supported by experimental evidence, they are not widely used in practice. One reason for that is the technical complexity of fitting PDEs to the experimental penetration data. This does not deter us from formulating the numerical portion of our later presented numerical model is a similar manner. the results of experiments performed using the afformentioned digital video analyses provide the necessary basis for our system specific assumptions when modeling the two physical systems. We also examine an alternative approach for describing the penetration process and experimental data treatment. The key idea is that the diffusion rate is mainly controlled by the resistance of the polymer matrix to the solvent flow, which is put forward in the molecular sorption model proposed by Vesely [63, 64]. This model visualizes the polymer matrix as a porous media containing voids filled by the solvent with the molecular interactions between the polymer and solvent molecules resulting in an internal pressure, similar to the capillary pressure. Thus, the penetrant motion is driven by the capillary pressure with the contact angle opposed by the viscous resistance forces.

Chapter 3

Tablet Dissolution and Disintegration Characterization

Drug product dissolution testing is of critical importance in pharmaceutical development and manufacturing. The development of new formulations are often guided by their subsequent in-vitro dissolution performance. Furthermore, in-vitro dissolution performance is an FDA requirement for manufactured drug batches. While the validity of dissolution experiments utilizing the USP II appartus has been called into question[65, 66], it continues to be the most used dissolution assay in industrial pharma. As such we have implemented it use in our studies of tablet performance.

3.1 Solvent Penetration

In order to determine a bulk rate of solvent penetration for the system, a modified computer vision analysis will be performed which tracks the penetration of solvent into the tablet matrix in 1 dimension as a function of time. The experimental setup consists of a GimaGo 470C GigE ethernet camera connected to a Windows 7 PC with an Athlon Phenom II quad core processor and 8gB of 1667MHz DDR3 ram and a Western Digital Raptor 15K rpm hard disk drive; Nikon Macro lens; halogen lighting system; and Agilent micropipette as shown in Figure 3.1. Videos are made of tablets as a predetermined(usually 50-100μL of deionized water at 37.5°C) volume of fluid is deposited atop the tablet in a single dose. Once the videos have been made of the tablets, a custom python script is used to analyze the front location as well as the movement of the top surface to determine the subsequent solvent penetration rate and swelling response. These values will later be used in the numerical modeling of the dissolution. For our purposes, special compactions of the two extreme processing conditions were selected for this battery of experiments, 40rpm-40rev and 160rpm-640rev as these are expected

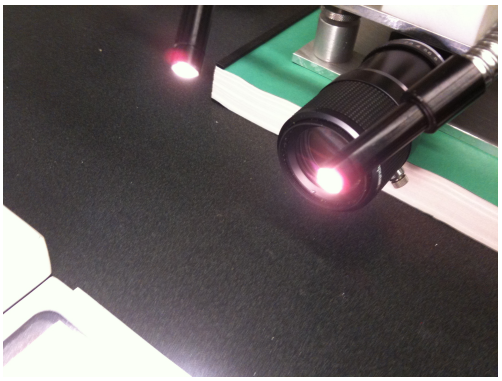

(a) Camera and Lighting Setup

(b) Macro Lens

(c) Micro-pipette

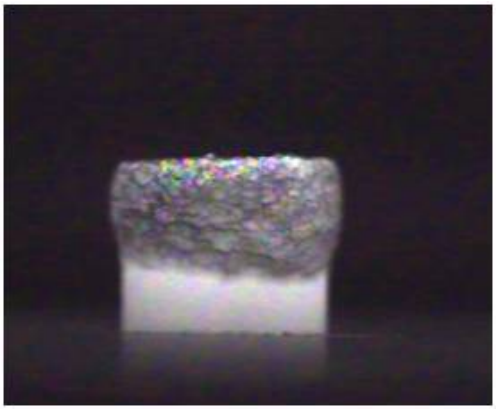

(d) Swelled Tablet

Figure 3.1: Figure shows components involved in the solvent penetration analysis.

to be the most different in terms of performance. The blends are compressed using a Presster tablet press simulator set to model a Kikisui Libra2 press moving at 60rpm. 10mm, round, flat face, B-type, D2 steel tooling (Natoli Engineering Co., Inc.) is used. Tablet mass is 405mg±3mg and compaction force is either 8kN±.4kN or 13.8kN±.4kN. Precompaction force is minimal, and kept below 1kN. A set of compaction curves are produced by making tablets of each blend at multiple compaction pressures and then measuring mass (balance portion of Pharmatron Auto Test 4), thickness and diameter (Mitutoyo Digital Calipers, CD-6"CX) and hardness (Pharmatron Tablet Tester 6100D). To monitor the penetration distance, we perform simple experiments by carefully depositing 75L (for Chlorphen tablets) of distilled water in the center of the top surface of the tablet using a metered micropipette. (Eppendorf Reference model E2000-100 with disposable tips) The amount of water is chosen so that it does not flow over

the side of the tablet, but still creating conditions where a high concentration remains on the top surface until the solvent interface penetrates about half of the tablet thickness, approximately 2-3 mm. This is done to ensure solvent penetration progresses exclusively through the top face of the tablet, effectively reducing the experiment to a one-dimensional characterization. For the hand pressed DCL14SD tablets, this experiment is performed approximately one hour after the tablets are compressed. All tablets are measured for mass, thickness and diameter (same equipment as previously described) immediately before performing penetration tests. Sample size for each group is 8 tablets, except for the high compression force Chlorphen tablets which have a sample size of 4. To film the penetration we use a GimaGo GO443C camera positioned to capture the cylindrical side wall of the tablet. Figure 3.2a shows a typical sequence of collected images. The GimaGo camera is connected via Cat-5 cable to the network card of a desktop computer running Windows7. Videos are captured and stored using the Xvid codec. We use the OpenCV [67] computer vision library in Python to extract the interface position with time from the collected images comprising the videos as follows. First, the color images are converted to grayscale, and a rectangular area with a width of about 200 pixels along the tablet thickness is selected for analysis, as shown in Figure 3.2b. Then, the average pixel intensity over the width of the chosen area is calculated and the noise is eliminated from the resulting curve using smoothing splines. Finally, edge detection of the first and second derivatives defines the position of the interface as seen in Figure 3.2c. The described algorithm was programmed and can run, in principle, in batch mode to process many images at once. We noticed, however, that different images require varying degree of smoothness for the noise elimination. Thus, in order to ensure a more accurate capturing of the interface position, we performed the smoothing step interactively and checked the results with visual inspection of the images periodically.

To validate teh effectiveness and repeatability of the technique, we perform an analysis of tablets composed of directly compressible lactose (DCL), specifically SuperTab 14SD obtained from DMV Fonterra. This material is chosen as the particles are generally spherical in nature and exhibit a relatively narrow particle size distribution. The

tablets are to serve as a validation of the technique which will subsequently be used to analyze tablets prepared from the Chlorphen blends. The DCL tablets are prepared using a custom manual hydraulic press comprised of an Enerpac P392 hydraulic hand pump and cylinder which actuates a steel stage from the bottom and a Delta Metrics XLP58-020K force transducer located above the moving stage. An LCD display shows the current force being registered by the transducer at all times during the compaction process. In order to ensure the outer surfaces were free of imperfections and that no lubricant would be necessary in the DCL powder, tablets are compressed at much slower speeds than could be readily achieved using a rotary tablet press or simulator. Attempts to use either of these alternate platforms resulted in tablets shattering upon ejection. A 10mm flat faced punch and die set made of polished S7 steel is used. Each tablet is made by weighing out 400mg±4mg of DCL on an Ohaus digital balance. The filled die is placed in the hydraulic press and the pump operated until the target force is reached. The actual compression takes place over a period of approximately 10 seconds, and the applied force is held constant for 10 seconds before the pressure is released. As the press is manually pumped, the exact time of the compression event cannot be controlled, however, it occurs at a speed which is sufficiently slower than the assumed relaxation time of the powder such that the compaction process can be assumed equivalent for each set of tablets. Once the powder is compacted, the die is placed on top of a hollow cylinder inside the press and pressure reapplied until the tablet is released from the die. The force required to remove the tablet was never greater than 1kN. After removal of the tablet, the die set is cleaned with water, then methanol and wiped dry before reuse. The resulting tablets are examined to ensure the surfaces are defect free, then weighed and measured for thickness and diameter. Any tablet which falls outside of the prescribed tolerances of mass (400mg±4mg) or thickness (4.00mm±0.05) is discarded immediately. Six tablets are selected from those produced in the hydraulic press for hardness testing. These tablets are allowed to rest for about one hour after compaction before measuring mass (balance portion of Pharmatron Auto Test 4), thickness and diameter (Mitutoyo Digital Calipers, CD-6”CX) and hardness (Pharmatron Tablet Tester 6100D).

3.1.1 Experimental Results

The DCL tablets have an average tensile strength of 0.91 MPa tensile strength with a standard deviation of .0089MPa at the compaction force of 4kN(51MPa compaction pressure). This is just under 1% of variability. This data combined with the acceptance of only tablets which fell within specified criteria allows us to assume the remaining DCL tablets are sufficiently similar in terms of physical properties. Figure 3.4 shows the measured penetration distance data for tablets compressed with the compression force of 4kN. The curve is initially fairly linear, but decays over time. This decay may be the result of several factors, such as the decrease in concentration of fluid as it is spread over a larger volume or dissolution of lactose into the water changing its chemical composition or physical properties. We do not explore the exact nature of this decay in this work. Of particular note is the consistency of the penetration results. The standard deviations are small as compared to the magnitudes of the measurements. As the tablets examined are composed of a single component and prepared in an identical and repeatable manner, the variability of the technique is minimal, and differences in measurements between future, less identical, samples is most likely due to differences in the samples as opposed to noise in the measurements. Figure 3.4 shows the best fits of these two models to the solvent penetration results from the DCL tablet experiments. The molecular sorption model appears to provide a rather high fidelity fitting of the results, well within the experimental error. By contrast, the Washburn model does not fit within experimental error. The initial slope of the Washburn model causes the fit to deviate from the experimental results and it is unable to overcome this deviation until much later.

3.2 Physical Dissolution

The USP II apparauts we utilize is a Vankel VK7010 USP II dissolution system attached to a Cary 50 Bio UV Visible Spectrophotometer (Varian Medical Systems, Inc.) equipped with quartz flow cells. This unit consists of standard bell shaped glass dissolution baths which are filled with 900 mL of distilled water at 37.5 C. The fluid in

the baths is stirred using paddles, which are rotated at 75 rpm. Samples are taken every 3 minutes. This consists of 2mL of fluid being automatically transferred to the flow cells from all vessels simultaneously. The flow cells are then individually scanned using UV spectroscopy. Once all cells are scanned, the fluid in the cells is returned to the dissolution vessels simultaneously. Testing is performed for six samples from each batch.

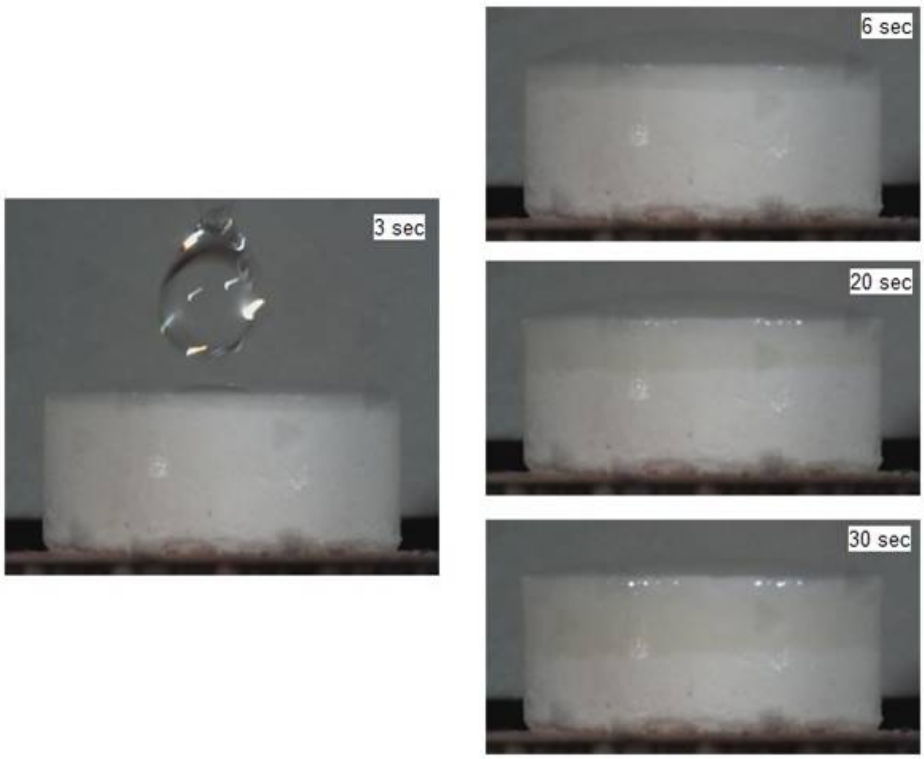

(a) Solvent penetration experiment sequential images

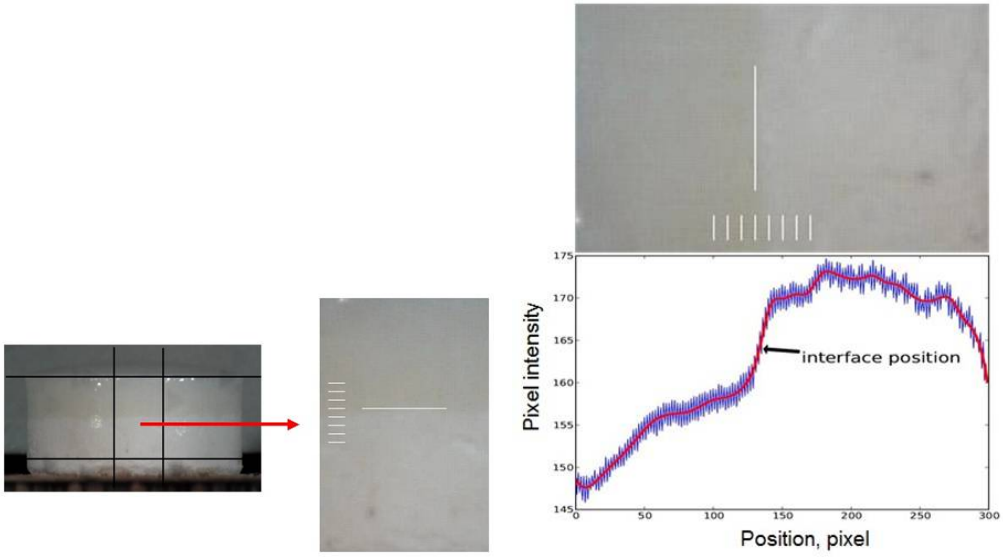

(b) Portion of image selected for analysis

(c) Smooth spline representing image

Figure 3.2: Steps involved involved in the solvent penetration analysis.

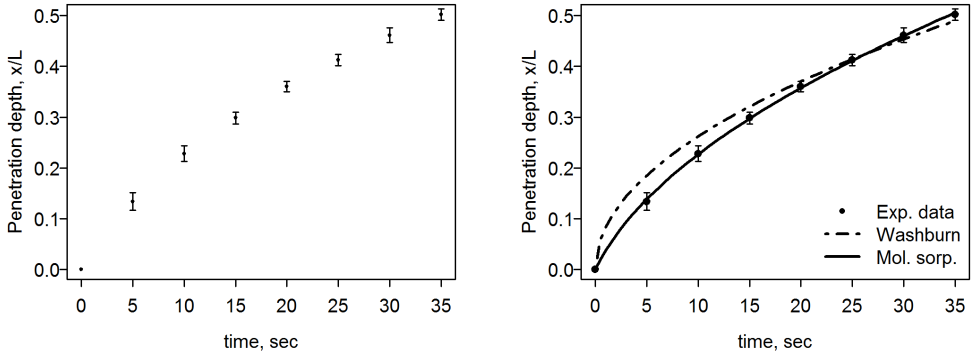

(a) DCL solvent penetration experimental results

(b) DCL solvent penetration model fit

Figure 3.3: Experimental results of solvent penetration and resulting model fit for both Washburn and molecular sorption

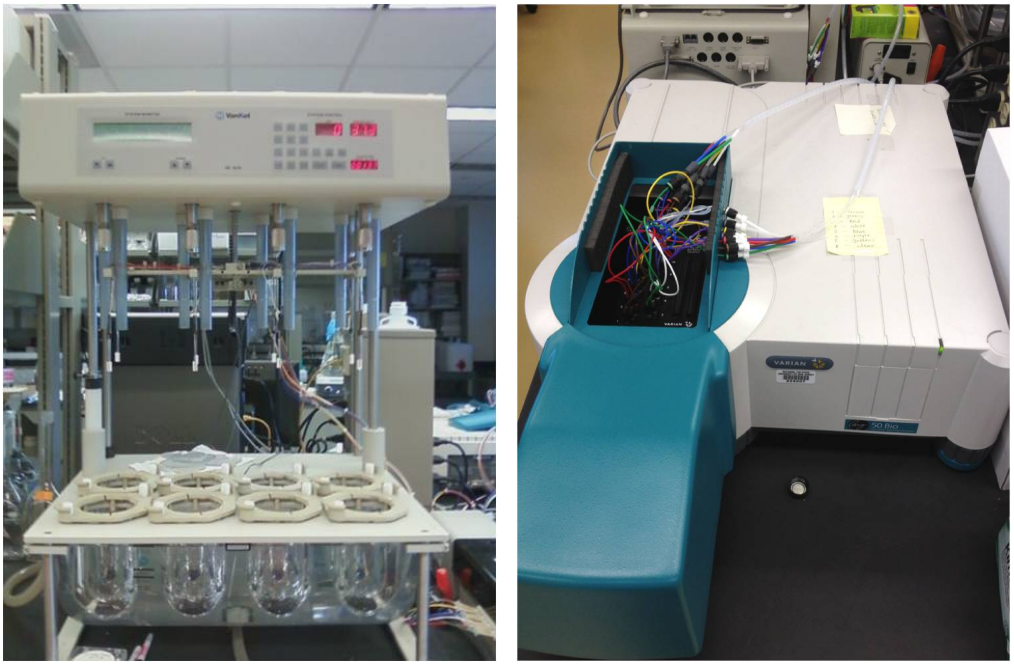

(a) Dissolution bath apparatus

(b) UV spectrometer

Figure 3.4: Experimental apparatus used in dissolution assays.

Chapter 4

Modeling Framework

When a pharmaceutical tablet is ingested a set of processes occur which results in the release of the active drug component. Once the tablet has reached the stomach, unless there is an enteric coating, the surface of the tablet immediately begins interacting with and absorbing the surrounding fluid. As the excipient matrix absorbs the fluid, active drug particles are dissolving inside this now wetted matrix. The resulting drug solute then diffuses out past the tablet surface until it reaches the surrounding bulk fluid and becomes mixed. In more complex physical cases the excipient matrix can swell and/or fracture resulting in movement of the tablet surface and the formation of new interfaces. A side by side comparison of the different processes we consider is shown in Figure 4.1 with time based progression.

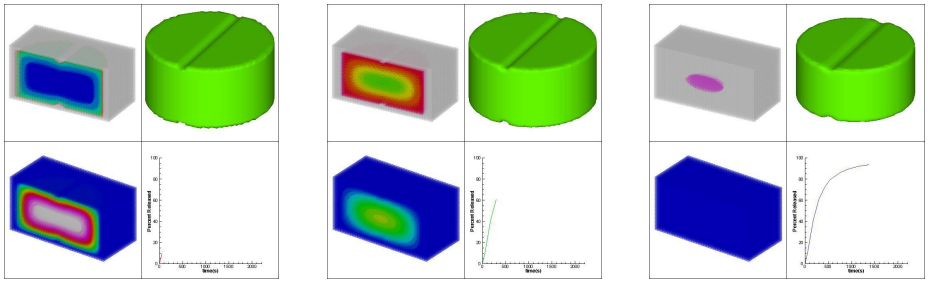

(a) 60s (b) 300s (c) 1380s

Figure 4.1: This figure shows the progression of a specific tablet dissolution model in four ways. From top left moving clockwise; API concentration, tablet/bulk fluid interface, release profile(percent released vs. time) and solvent concentration.

A physics based model including each of these processes in a 3-dimensional framework has been developed and tested[68]. The model system incorporates results from physical experiment data and in-silico models of die filling and compaction to define

tablet models to be simulated in a defined environment. The distribution of components and microstructure will influence the solvent penetration and dissolution/diffusion of active material with the goal being to determine the effect of formulation and processing changes on product performance. Ideally this performance analysis will enable the model to produce predictive results for similar tablets.

4.1 Numerical Scheme

4.1.1 Moving Boundaries

One of the primary concerns of the numerical simulations is proper evolution of the tablet fluid interface. Previous work has shown scaling between identical formulations compacted in different geometries[16]. There are numerous schemes which have been developed, both Lagrangian and Eularian, to track changes of a surface. As the problem of tablet dissolution entails tracking complex geometry changes based on various external and internal effects, it is important to use a surface tracking method which is both stable and inexpensive. Lagrangian methods often rely on complicated meshes which are adapted over time. This remeshing can result in a highly distorted grid shape, which can in turn negatively influence the time-step which is based on the smallest grid size. The simplicity and consistency of fixed-grid method has focused our attention on Eularian methods. The most commonly used Eularian methods of surface tracking are the Volume-of-Fluid method by Hirts and Nichols, the phase-field method and the level set method by Osher and Sethian. Level set functions have been shown to produce smooth evolution of surfaces with complex geometry and are extremely well suited for use on cartesian based grid structures. There has been extensive work[69] employing levels sets to track surfaces for the purpose of modeling fluid dynamics, crystal growth and chemical deposition. The ability of level sets to operate based on a single velocity function makes this framework easy to expand as well, since all of the effects considered can be combined into a single function representing the velocity of the surface. Inclusion of additional factors will have no effect on the level set implementation and can be incorporated directly into the velocity function. In addition, the formation of

new surfaces are handled implicitly by this function, which will become important as the internal effects of swelling are added to the model and fractures and cracks develop. The methodology used was adapted from a framework developed by Kinjal Dhruva[70]. The implementation is similar to that used by Javierre et al.[71]

4.1.2 Solvent Penetration

An important factor in tablet dissolution is the penetration of solvent into the excipient matrix. In the physical process of dissolution, the surrounding solvent enters the excipient matrix of the tablet similar to a sponge soaking up water. While the process of solvent entering the tablet takes longer than water entering a sponge, the process by which both happen is very similar. The small voids between particles in a tablet allow for water to enter and proceed through the tablet, in many cases, to the center of the tablet. As the tablet enters the solvent media, or after the simulation is started, the tablet begins to soak up the surrounding fluid. In many cases this will result in the tablet swelling and possibly fracturing. While the present iteration of the numerical simulation does not incorporate swelling or fracture, the bulk fluid is still considered to penetrate the excipient matrix. Solvent penetration is represented as a diffusion based process, whose rate is manipulated via a diffusion coefficient which represents the porosity, hydrophobicity, and tortuosity of the compacted particles. The method is based on Fick's second law, and incorporates the effects of a non-uniform diffusion coefficient:

$$\frac{\partial C_w}{\partial t} = \nabla . \alpha_w \nabla C_w \tag{4.1}$$

This equation can be expanded in one dimension using the chain rule to:

$$\frac{\partial C_w}{\partial t} = \frac{d\alpha_w}{dx}\frac{dC_w}{dx} + \alpha_w \frac{d^2 C_w}{dx^2} \tag{4.2}$$

Where:

C_w is the concentration of solvent

$C_w = 0$ at $\phi = 0$, the tablet/bulk fluid interface

t is the time in seconds

α_w is the penetration/diffusion coefficient. This value is assigned at initialization, and can vary throughout the tablet.

x is the position in the x direction

Full expansion results in a summation of the right side of the equation for all included dimensions, in our case x, y and z. The incorporation of a non-uniform diffusion coefficient allows for better tablet definition especially when exploring the effects of channeling. The prescribed diffusion coefficient represents the aggregate effects of porosity, hydrophobicity and tortuosity of the excipient matrix. Since physical tablet structure may not have uniform porosity, the function is so defined that each cell represented has its own solvent diffusion coefficient. This diffusion coefficient represents a combination of the physical factors affecting the rate of solvent entering the tablet. The variation of α_w is explored later in the paper. It has been argued that solvent penetration into a polymer matrix would be better represented by Case II diffusion, but in the case of the referenced physical experiments, solvent penetration of the tablets would best be described as anomalous diffusion[3, 72]. While this is still not the exact solution, it is a quick way to get useful results. Some early simulations were performed showing the effects of the different diffusion types on the model output was nominal at relatively fast penetration rates. As this was the case, Case 1 diffusion was implemented for the simulations as this reduced the number of variables to be estimated. The progression of the solvent through the excipient for a specific model is shown in Figure 4.2. At the onset of the simulation, the tablet is assumed to be completely dry, and everywhere outside the tablet is pure solvent. The representative initial conditions assign a value of 0 to all nodes inside the tablet and a value of 1 to all nodes outside the tablet. As the simulation progresses, the value of a node inside the tablet can increase until it has also reached a preset maximum. This represents full saturation of the corresponding volume of the tablet. The external concentration is held constant at 1, as it is assumed the tablet is surrounded by pure solvent. There is a slight exception to this rule for the set of nodes located just outside the surface. These nodes are assigned

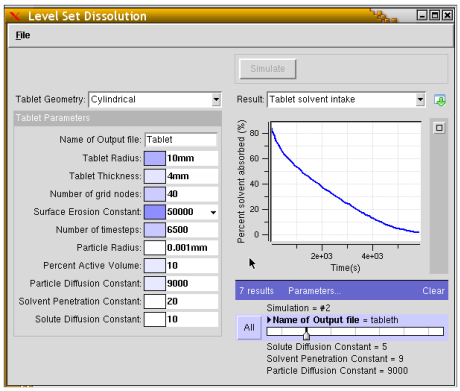

Figure 4.2: Graph represents dryness of model tablet. Scale is from completely dry(100) to completely wet(0). This result is from a simulation with no swelling, comparatively slow uniform surface erosion, and models solvent penetration using Case 1 diffusion. The resulting API dissolution progress for this same model is presented in the next figure.

a temporary concentration using the ghosting method previously outlined in the level set section. This temporary concentration is greater than 1 so as to properly represent a concentration of 1 at the surface of the tablet. By increasing the concentration of solvent at these surrounding nodes, the error associated with grid size is reduced, and the resulting evolution is more meaningful. A more complex model based on the diffusion equation has also been generated and implemented. This case incorporates the effect of changes in porosity due to dissolution of active particles in each cell.

$$\frac{\partial \overline{C_w}}{\partial t} = \nabla . \frac{\alpha_w}{\epsilon^2} \nabla \overline{C_w} \epsilon \tag{4.3}$$

This equation can be expanded using the chain rule to:

$$\begin{aligned}\frac{\partial\overline{C_w}}{\partial t} = \\ &(\frac{\partial\alpha_w}{\partial x}\epsilon^{-1}\frac{\partial\overline{C_w}}{\partial x} + \alpha_w\epsilon^{-1}\frac{\partial^2\overline{C_w}}{\partial x^2} - \alpha_w\frac{\partial\overline{C_w}}{\partial x}\epsilon^{-2}\frac{\partial\epsilon}{\partial x}) \\ &-(\frac{\partial\alpha_w}{\partial x}\epsilon^{-2}\frac{\partial\epsilon}{\partial x} + \alpha_w\epsilon^{-1}\frac{\partial\overline{C_w}}{\partial x}\epsilon^{-2}\frac{\partial\epsilon}{\partial x} - 2\epsilon^{-3}\frac{\partial^2\epsilon}{\partial x^2}) \\ &+(\frac{\partial\alpha_w}{\partial y}\epsilon^{-1}\frac{\partial\overline{C_w}}{\partial y} + \alpha_w\epsilon^{-1}\frac{\partial^2\overline{C_w}}{\partial y^2} - \alpha_w\frac{\partial\overline{C_w}}{\partial y}\epsilon^{-2}\frac{\partial\epsilon}{\partial y}) \\ &-(\frac{\partial\alpha_w}{\partial y}\epsilon^{-2}\frac{\partial\epsilon}{\partial y} + \alpha_w\epsilon^{-1}\frac{\partial\overline{C_w}}{\partial y}\epsilon^{-2}\frac{\partial\epsilon}{\partial y} - 2\epsilon^{-3}\frac{\partial^2\epsilon}{\partial y^2}) \\ &+(\frac{\partial\alpha_w}{\partial z}\epsilon^{-1}\frac{\partial\overline{C_w}}{\partial z} + \alpha_w\epsilon^{-1}\frac{\partial^2\overline{C_w}}{\partial z^2} - \alpha_w\frac{\partial\overline{C_w}}{\partial z}\epsilon^{-2}\frac{\partial\epsilon}{\partial z}) \\ &-(\frac{\partial\alpha_w}{\partial z}\epsilon^{-2}\frac{\partial\epsilon}{\partial z} + \alpha_w\epsilon^{-1}\frac{\partial\overline{C_w}}{\partial z}\epsilon^{-2}\frac{\partial\epsilon}{\partial z} - 2\epsilon^{-3}\frac{\partial^2\epsilon}{\partial z^2})\end{aligned} \tag{4.4}$$

Where:

$\overline{C_w}$ is the volume of solvent normalized to the volume of a cell(0(dry)-1(pure solvent)

t is the time in seconds

α_w is the penetration/diffusion coefficient. This value is assigned at initialization, and can vary throughout the tablet.

ϵ is the normalized porosity of a given cell(0(solid)-1(empty))

x, y and z correspond to the three physical dimensions

The maximum volume of solvent in a given cell is limited by the total porosity (void or non-solid fraction) of that cell.

4.1.3 Active Dissolution

Particle dissolution is calculated using a set of parameters which represent the average values of particle size, shape, and concentration for each cell. The size, shape and number of active particles is initially defined for every cell located inside the tablet. At the beginning of the simulation, each grid cell inside the tablet is assigned a number of active particles of known size. The number and size of the active particles is used to produce a volume based concentration of active particles. While the concentration flux is determined based on the bulk active concentration of each cell, the volume of

the individual particles is considered to decrease with this bulk concentration. This results in a decrease in surface area of the particles which affects their bulk dissolution rate. The representative equation is similar to the Brunner equation[11], but takes into account the inability to properly measure a diffsuion boundary layer around individual particles. Recent work by Brasseur[73] has shown a constant definition of the boundary layer thickness is incorrect. We do not explicitly represent the boundary layer thickness, but instead employ a dissolution coefficient which is representative of the system specific dissolution rate. Surface area of particles and local solvent concetration are still handled explicitly.

$$\frac{\partial C_a}{\partial t} = \alpha_C (C_s - C_a) \tag{4.5}$$

Where:

C_a is the volume based concentration of active particles

C_s is the solubility of active in the fluid

$\frac{\partial C_a}{\partial t}$ becomes the "source" term for the solute diffusion equation in the next section

t is the time

α_C is the dissolution coefficient which accounts for the effects of surface area, solvent concentration, and a solvent/solute specific coefficient

$\alpha_C = \alpha_{API} S_p C_w$

S_p is the surface area of the particles

C_w is the normalized volume based concentration of solvent

α_{API} is the dissolution coefficient of the specific API or excipient/solvent system being considered. It is an assigned value which represents the affinity of the API to enter solution.

The diffusion boundary layer is not explicitly represented, but is considered to be a part of the coefficient α_{API}. Although the concentration flux calculations are made using the bulk concentration of each cell, the evolution of the individual particles is still considered. As the concentration decreases, the size of the particles in each cell

must also decrease. The change in API concentration is used to update the remaining volume of API in each cell and in calculating the contribution to the local solute concentration. Solute concentration will be further explained in the next section. This equation assumes that the active particles remain in the grid cell in which they were initially defined. That is not to say that solid drug particles are not be able to move in dissolving tablets, simply that such an effect is not handled via this particular model. In decreasing the volume of the individual particles in a cell, we assume that all of the particles of a given size in that cell dissolve at the same rate. Therefore in a monosized active distribution, all of the active particles in a given internal cell will be reduced by the same volume. This reduction in volume has a large effect on the rate of dissolution as the dissolution coefficient takes into account the surface area of the particles. In this equation, α_C is determined by three factors; combined surface area of active particles in the cell, solvent concentration in the cell and an active ingredient/solvent system based dissolution constant. This results in a diffusion coefficient which can change not only based on the location inside the tablet, but also with every timestep. As time progresses the concentration of active particles decreases and particle volume is reduced until the particles in a cell have decreased below a threshold volume. Once the particles in a given cell have reached the threshold volume, they are then considered completely dissolved and are removed from the simulation. Figure 4.3 shows the resultant concentration distribution of a model after 6500 iterations.

This procedure is also applicable to discretely represented particles. In the case of a discrete particle representation, the reduction in volume of each particle is also handled discretely. The solute and solvent concentration used for each particle is that of the cell in which the center of the particle is located. In addition, the amount of drug released at each time step from all of the particles in each cell is calculated simultaneously to ensure solubility limits are not breached due to multiple solute contributions. The percent released from the dosage form is calculated at this stage. The reduction in volume of the individual API particles is compared to the initial particle volume distribution. The total mass of active material in the tablet matrix is calculated as the combination of solid api particle mass and mass of solute. The ratio of the mass at a given time to the

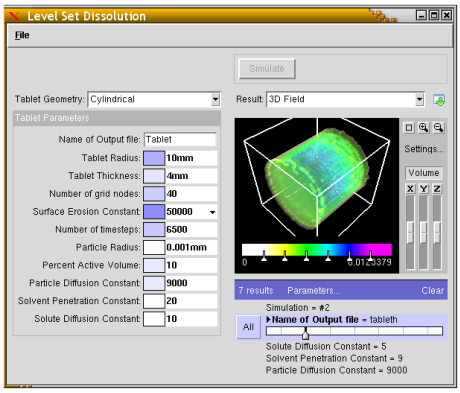

Figure 4.3: The image represents the remaining API concentration of the tablet after 6500 steps of iteration. This simulation was performed using Matlab on the Pharmahub servers of Purdue University. The tablet initially had a homogeneous dispersion of API, no swelling has taken place, erosion rate was uniform and comparatively slow, and solvent penetration was considered as Case 1 diffusion. This is the same model referenced in the previous figure in the Solvent Penetration section.

initial mass of drug is the amount released.

4.1.4 Active Diffusion

Once the active particles have entered solution the solute proceeds to diffuse out of the tablet and into the bulk solution. As the API particles dissolve, the associated volume of drug dissolved is converted to a solute concentration inside the tablet. This solute concentration must diffuse out of the excipient matrix to the bulk solution. The process is very similar to the solvent penetration into the tablet, and thus is handled in much the same mathematical formulation, save for the incorporation of its own constants, and the inclusion of a generation term.[74]

$$\frac{\partial \overline{C_s}}{\partial t} = \nabla . \frac{\beta_s}{\epsilon^2} \nabla \overline{C_s} \epsilon + \overline{C_a} \tag{4.6}$$

Where:

$\overline{C_s}$ is the volume of solute normalized to the volume of a cell and its specific solubility(0(empty)-1(full)

$\overline{C_a}$ is the normalized volume of API which has converted to solute form $C_s = 0$ at

$\phi = 0$, the tablet/bulk fluid interface

t is the time in seconds

β_s is the diffusion coefficient. This value is assigned at initialization, and can vary throughout the tablet.

ϵ is the normalized porosity of a given cell(0(solid)-1(empty/fluid))

x, y and z correspond to the three physical dimensions

Like the solvent penetration, the solute diffusion is solved using a modified version of Fick's diffusion equation4.4. Each cell inside the tablet represents a generating source, while the bulk solution outside the tablet is treated as a perfect sink. This assumption has been previously used and verified by Feldman in 1967 [12], and used by others since[22]. At every timestep the contributions from the particle diffusion step are added to the solute concentrations, then the solute concentrations are updated using a basic finite-differencing scheme like the solvent concentrations. Currently, the solute concentration is not directly used in determining the percentage of drug released from the tablet. This is calculated as the difference between the initial solid volume and the current remaining solid volume of API.

Chapter 5

Solid Oral Dosage Form with Diffusion Dominated Drug Release

5.1 Introduction

The simplest pharmaceutical tablets are made from directly compressible blends. Directly compressible blends are blends of excipients (including lubricants) and API which are prepared in a single bin blending step and then compressed. There are no other scheduled unit operations which take place before the powders become tablets. However, force feeders in many commercial tablet presses induce shear mixing. This mixing is generally unintended and can have effects on final product performance which can result in extreme changes in product performance[75]. Herein we examine a specific blend which exhibits shear sensitivity. Raw materials are blended in a traditional lab scale V-blender and then subjected to varying amounts of shear and a custom shear mixer. The effects of this shear on blend and tablet properties and performance are measured, evaluated and then using numerical models attributed to specific changes in blend and subsequently tablet microstructure.

5.2 Experimental

5.2.1 Base Materials

Pharmaceutical tablets are compacts of blended and processed powders. The complete production process can range from a simple blending in a single stage mixer, to high shear wet granulations which span multiple processing steps before reaching the compaction stage. The effect of processing, however, depends on the properties of the ingredients being utilized. The blends and tablets investigated in this chapter are made

from four ingredients:

Microcrystalline cellulose (excipient, MCC)

spray dried lactose (excipient, FFL)

chlorpheniramine maleate (model API, CH)

magnesium stearate (lubricant, MgSt)

Figure 5.1a shows a Scanning Electron Microscope (SEM) image of MCC particles

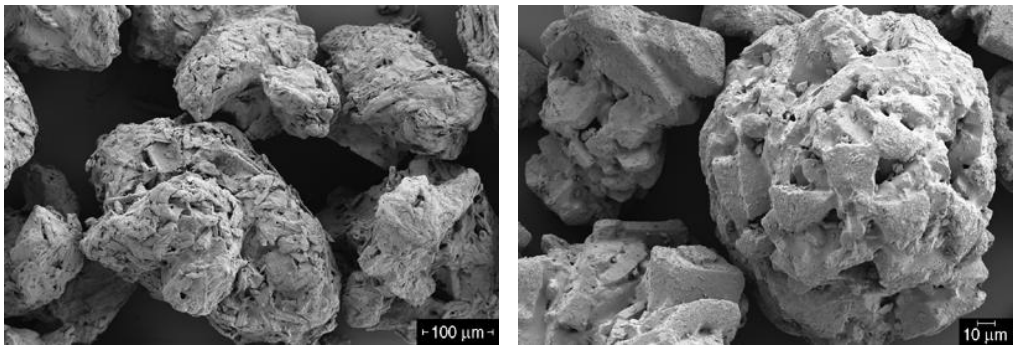

(a) Avicel PH200 (b) Fast-Flo Lactose

Figure 5.1: SEM images of MCC and FFL. MCC particles are rough and porous. FFL particles are spherical, but have surface pores whose diameters are of the order of 5-10 μm

similar to the ones used in our experiments. The particles are globular and have a rough and porous surface. The porosity of these particles is in large part the reason for their high compactibility. The lactose particles show a similar surface porosity, though the overall shape appears more spherical than the MCC particles.

5.2.2 Manufacturing

Mixing

In order to create samples for analysis, a 4 kg base blend was created containing Microcrystalline cellulose(45%, Avicel Ph200, MCC), Fast-Flo Lactose (45%, Foremost Farms), chlorpheniramine maleate(9%, model API, CH), magnesium stearate(1%, MgSt). The chlorpheniramine was sieved through a 100 micron metal mesh to ensure any agglomerates would be broken up before mixing. The cellulose, lactose and chlorpheniramine were mixed together in a V-blender(Patterson Kelley) for 15 minutes at

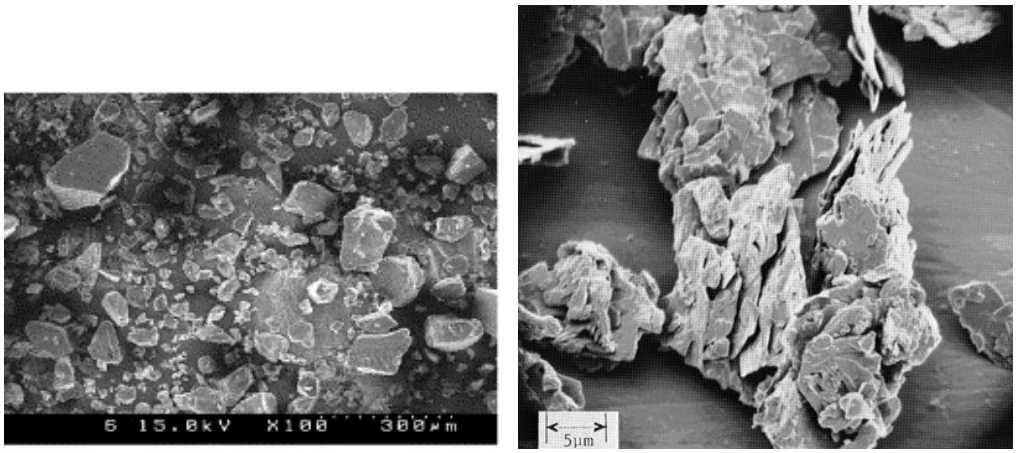

(a) Cab-o-Sil (b) MgSt

Figure 5.2: SEM images of Chlorpheniramine and MgSt. Chlorphen particles appear to be chunky and brick-like. MgSt Particles are agglomerates of platelets.

15 rpm. The MgSt was then added and the blender rotated for an additional 25 revolutions. This base blend is then parceled out into 15 300g batches which undergo additional mixing and shearing in a custom high speed shear rheometer. The shear rheometer allows for the controlled application of shear which might otherwise be induced by excessive blending time or intensity or a poorly deigned tablet press feed frame. Figure 5.3 shows the mechanical setup of the rheometer, which consists of a centrally rotating column with baffles facing outward, a cylindrical fixed shell with baffles facing inwards, and smooth faced top and bottom. The rotational speed is controlled by a digital input dial and the total strain is measured in terms of the total number of revolutions of the central cylinder. This is implemented by controlling the total operating time for each run based on the desired total strain and current speed setting. Powder was removed from the device by opening a dispensing gate on the bottom face and spinning the rheometer at 4rpm for 10 revolutions. Any powder left in the rheometer after this was vacuumed out and the rheometer cleaned using methanol and wipes before processing of the subsequent batch. The shear rheometer allows for work which might otherwise be imposed on a powder blend via an active tablet press feed frame to be performed in a controllable manner in a separate system. This is important in regards to the method of tablet compaction utilized herein. Tablets are

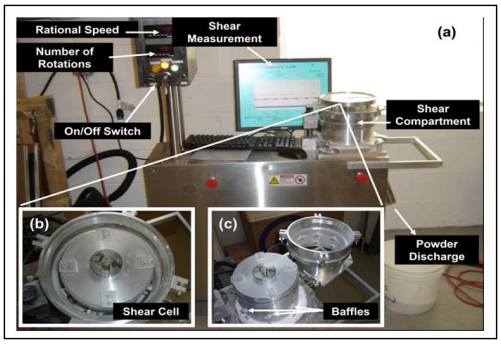

(a) High Speed Shear Rheometer

Blend #	Shear Rate(rpm)	Total Shear(rev)
1	40	40
2	40	80
3	40	160
4	40	640
5	80	40
6	80	80
7	80	160
8	80	640
9	160	40
10	160	80
11	160	160
12	160	640

(b) Table of shearing conditions

Figure 5.3: Figure a shows the physical shear rheometer setup. Figure b is a table of the shear conditions

compacted using the Presster®(Metropolitan Computing Corporation, East Hanover, NJ). The Presster®fills the tablet die using a gravity fed shoe which imparts neglible work to the powder blend unlike an active paddle based feed frame which shears and scrapes powder into the tablet dies during compaction.

Tablet Compaction

Once the prescribed sheared blends are complete, the tablets are made using a Presster®tablet press simulator. The Presster®is set to simulate a Kikisui Libra 2®45 station press, making tablets at a rate of 150000 per hour, or 25rpm, using a set of 10mm flat faced cylindrical punches made of S7 steel. Compaction settings are controlled to produce tablets of specific densities. As this is not a direct setting, the compression and dosing heights are adjusted specifically for each processed batch, and any tablets whose density falls outside the prescribed range is discarded immediately. Tablet target mass is within a tolerance of +/-5mg, and target density is within +/- 5%. Subsequently, compaction

curves are produced for the least and most processed blends; 40rpm-40rev and 160rpm-640rev. Figure 5.4 shows the compaction profile of both processed Chlorphen blends

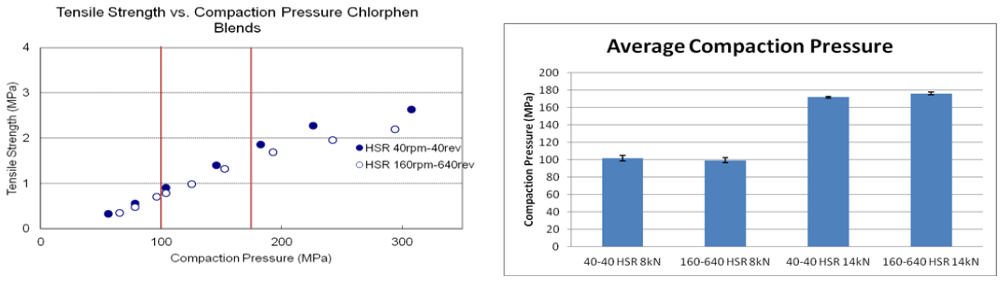

(a) Compaction curve Chlorphen blends (b) Chlorphen tablet tensile strengths

Figure 5.4: Compaction response and average tensile strength of Chlorphen tablets.

being investigated. At the lower compaction force (8kN, 100MPa pressure), the ratio of compaction pressure to tensile strength is very similar for both blends, however, at the higher force (14kN, 170MPa pressure) the difference in ratios is noticeable with the 640rev batch achieving less tensile strength at even greater compaction pressures. The differences in the compactability of the two blends is minor, especially in the range of compaction pressures used to produce the samples for dissolution testing.

5.2.3 Characterization

Tablets from each batch of powder are subjected to a battery of tests. Six tablets undergo LIBS analysis, and are then be used for hardness tests as the removal of powder via LIBS ablation does not affect bulk tablet hardness and both tests are technically destructive. An additional six tablets are reserved for dissolution in a USPII apparatus. Three tablets are used in the solvent penetration experiments. All tablet are measured for mass and thickness.

LIBS analysis

Six tablets from every batch are subjected to analysis using a Pharmalaser PharmaLIBS ®apparatus. The LIBS-based instrument(PharmaLIBS®, model 200), dedicated to pharmaceutical applications, purchased from Pharma Laser (Boucherville, QC, Canada). An interline readout CCD array detector allows gated detection of the

spectrum. The best sensitivity of the CCD camera was defined between 300 nm and 800 nm. The camera delay is set to 1.0 μs with an exposure time of 2.0 μs, and the binning group was set to 100. The environmental conditions in the lab at the time of sample acquisition were atmospheric pressure at 24°C. The tablets will be subjected to a sampling method which included laser power setting of 150mJ which produced pulses between 145 and 158mJ pulsed at 2 Hz at 31 sites for a total of 5 consecutive shots per site. Previous experiments have shown this results in an average overall sampling depth of 200 microns. Figure 5.5 shows the portion of spectrum collected for each shot, which also includes emission from the diatomic fragment of a broken carbon ring(referred to as C2). The magnesium signal is defined as the net peak height, i.e. the maximum intensity of the Mg(I)(magnesium, first ionization level) 518.36 nm line, minus the background signal. The C2 line was measured at 512.86nm. The plasma produced was imaged through a grating set at 1200nm centrally focused at 517nm with a full range from 507 to 527nm. The process is similar to that used by other groups researching the use of LIBS for pharmaceuticals [76]. LIBS analysis has shown a relation

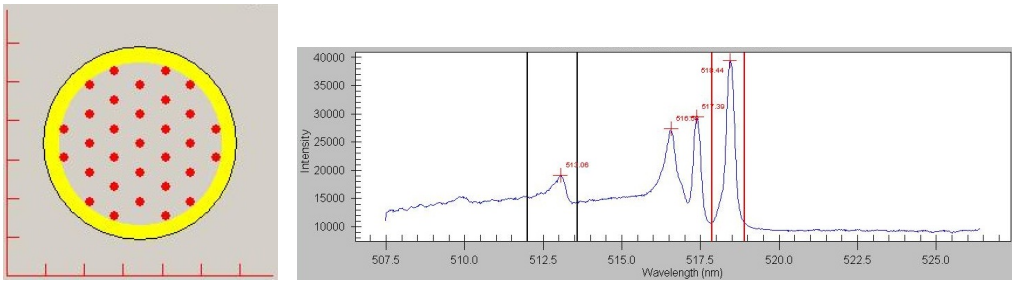

(a) Shot Stencil (b) Single Spectrum

Figure 5.5: Figure a shows the shot stencil which was used to analyze each tablet. Figure b shows a spectra from a single shot.

between the work input to the powder blend during processing and the signal intensity ratio of peaks representing ionic carbon(C2) and magnesium(Mg). This ratio decreases with every shot after the first. This could be a function of the volume being ablated at each shot, the propensity of the 2 materials to return to the ablated surface after the plasma cools or the propensity of Mg to migrate to the tablet surface as has been surmised in similar work[76]. It has become common practice, however, to ignore the surface layer of shots as well as the first shot at in each level as the values produced

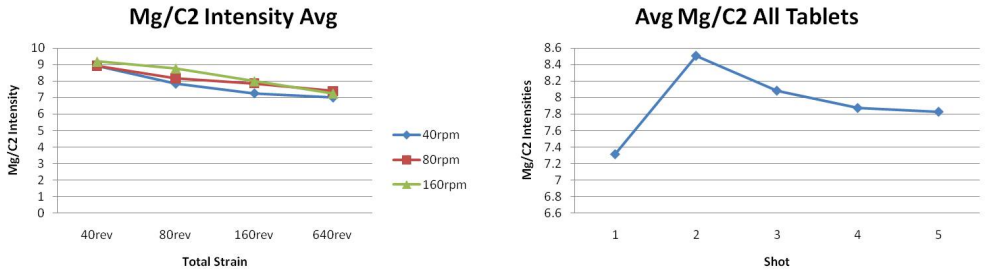

(a) Mg/C2 peak height (b) Mg/C2 average per shot

Figure 5.6: Figure a shows the batch average of the relative peak heights of Mg and C2. This value decreases with increased total strain. The average Mg/C2 ratio decreases with each shot.

are considered to be outliers caused by contamination of the sample or known issues with the laser and imaging system. MgSt peak height RSD decreases with increasing homogeneity. Current understanding of the powder system indicates that as total strain is increased so is the overall homogeneity of the blend. Fitting with this theory, the average C2 peak height RSD also decreased, with the exception of one case. The

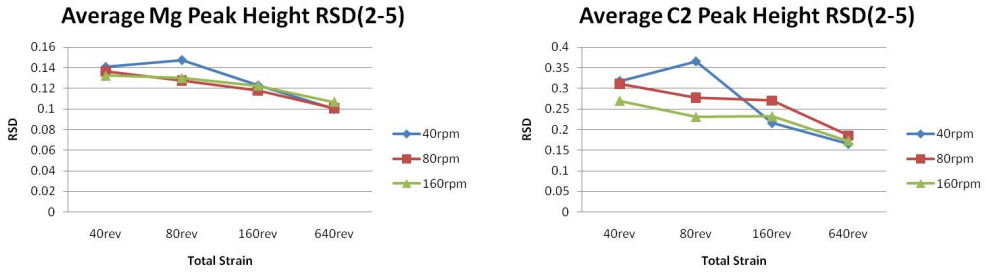

(a) Avg Mg RSD (b) Avg C2 RSD

Figure 5.7: The graphs show the batch average RSD for measurements of C2 and Mg peak height. These values ignore the first shot at each site.

peak intensity RSDs provide a good check for the peak height ratio technique. The RSD technique requires a large number of sites per tablet to be analyzed to insure accuracy, it is our hope through further examination to show the peak height intensity can provide acceptable characterizations of processing work input to the powder blend with relatively few shots. The 2-D images in Figure 5.8 provide a visual representation of the data collected from LIBS experiments. These images were created using the C2 peak heights at each site analyzed in single tablets. The value at each shot location is interpolated to produce a continuous field of component concentration. Tablets which

have undergone less shearing can have visible areas of higher concentration, "chunks", of API material, manifested as single shots with relatively high C2 intensity values and multiple contiguous shots with slightly elevated C2 intensity values.

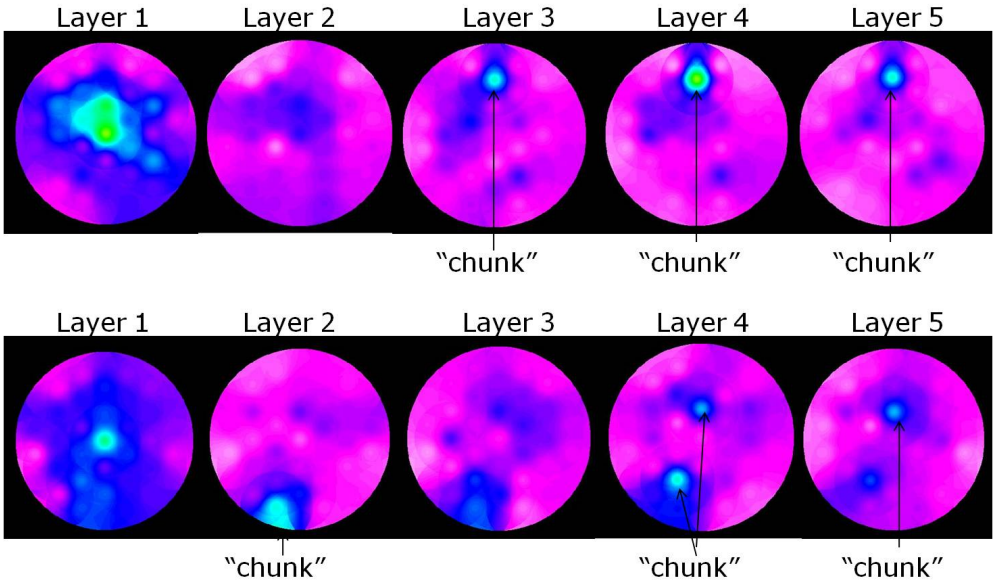

(b) Low Strain 2-D slices

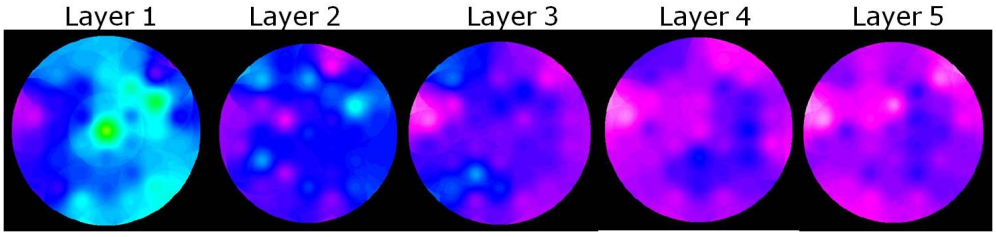

(c) High Strain 2-D slices

Figure 5.8: Images representing distribution of API in tablets. Tablets with more strain show more homogeneous distribution of API.

X-ray Tomography

As part of the LIBS experiments, X-ray tomography of post ablated tablets was used to determine the amounts of material which had been analyzed at each sample point. X-ray μCT analyses were performed using a Skyscan®1172 X-ray-computed microtomograph (Skyscan), imaged with an X-ray tube (voltage, 50 kV; current, 100 A) and a 0.5 mm aluminum filter. Pixel size was 13.4 μm and scanning was initiated from above the top of each tablet to at least halfway through the total thickness. For each

sample, 200 section images were reconstructed with NRecon software (version 1.4.3, Skyscan). Figure 5.9 shows a single slice of the tablet after reconstruction. The images produced by the tomography could not effectively be made into a 3-dimensional model, and, consequently, the comparisons were relegated to a simple depth analysis which was performed manually on select tablets. These images were processed by inspection and the depth of each hole was determined by the number of frames in which it was visible. Similar analysis of shot hole diameter was impractical due to the clarity of the images. At least 4 sites were measured for each shot depth except for the 1-shot locations which had a minimum of 2 sites measured. The results are visible in graphical form in Figure 5.10. The graph of shot depth standard deviation vs. number of shots

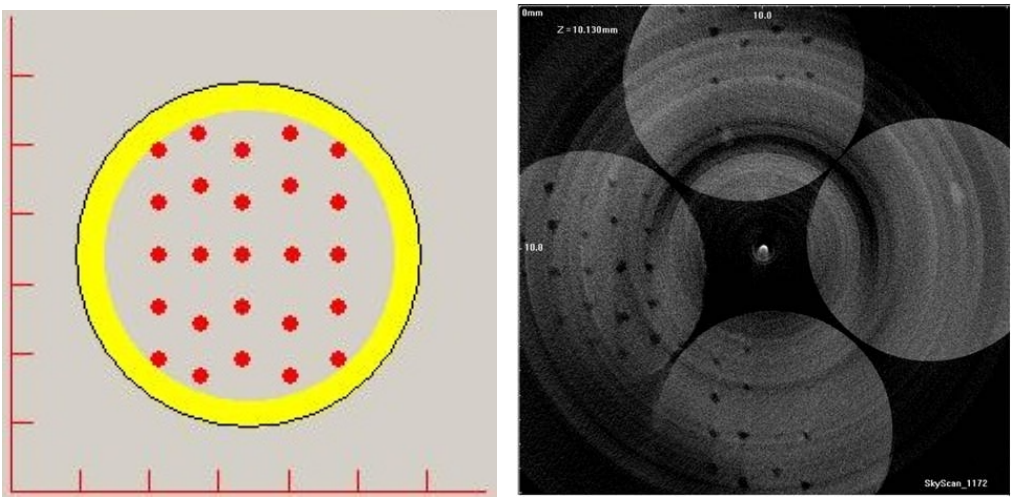

(a) LIBS depth test stencil (b) X-ray Image

Figure 5.9: Shot layout and reconstructed image slice from X-ray μCT depth analysis

in Figure 5.10 shows how much of an effect the matrix properties can have on what is being analyzed. The large changes, especially for the 4 shot group, show that additional tweaks are needed to accurately quantify the readings from the samples. The tablets which underwent a greater amount of total strain, and were therefore considered to have a more homogeneous distribution of materials, showed a more consistent decrease in depth than the less homogeneous tablets. Older works have attempted to quantify matrix effects, or the role of the microstructure on the imaging results[47, 77], but the concept still remains poignant in recent works[78]. The technique we previously used will be adapted to increase the quality of the images produced with the goal of creating

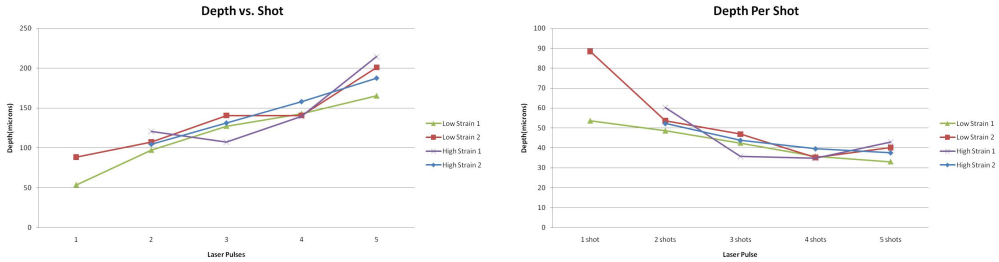

(a) X-ray Depth vs. Shot

(b) X-ray Depth per Shot

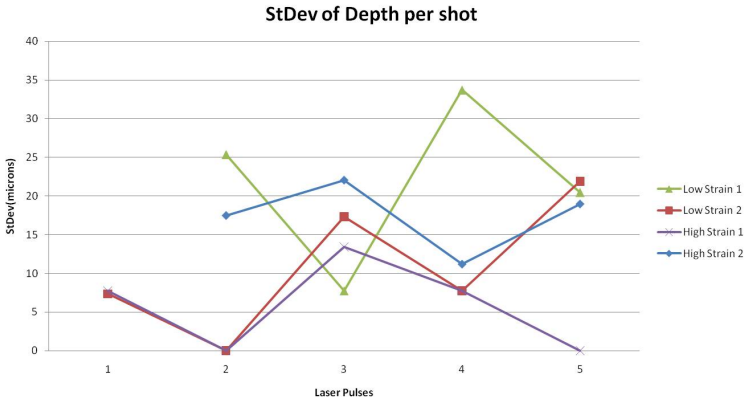

(c) X-ray StDev vs. Shot Depth

Figure 5.10: X-ray μCT depth analysis results.

useable 3-dimensional reconstructions to more easily and accurately measure the resulting volume of multiple ablations. Tablets of interest will be "sandwiched" between unablated tablets of the same material and conditions and then leveled relative to the X-ray detector. This will hopefully reduce the exagerrated "ringing" effect produced at the tablets' top surface in the previous attempts.

5.2.4 Dissolution

Tablet dissolution is performed on six tablets from each blend at each compression condition. Experiments are carried out using a Varian Vankel automated eight bath dissolution system as shown in Figure5.14a. The six 900 mL baths used for samples are filled with distilled water at 37.5°C, and paddles rotated at 75rpm. The remaining two baths are filled with a blank and a standard solution. Sample measurements are made

using a Varian UV spectrometer(insert actual name here) equipped with autosampler and flow cells, Figure5.14b and c. Samples are taken from each of the eight baths at time zero and then every three minutes until the allotted testing time has concluded. An analysis of the average dissolution rates of tablets from different blends, Figure 5.12,

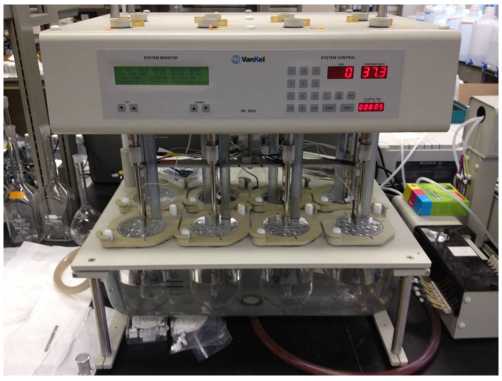

(a) Varian dissolution bath setup

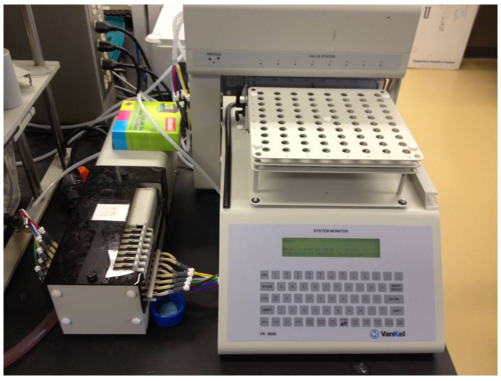

(b) Autosampler

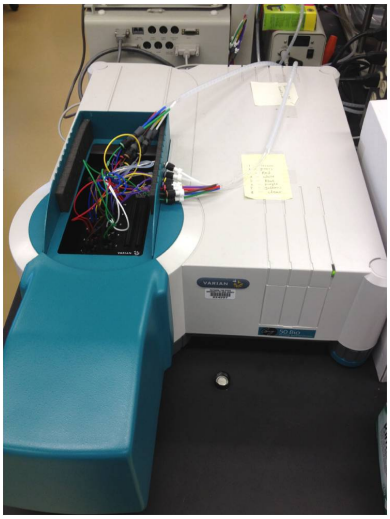

(c) UV spectrometer and flow cells

Figure 5.11: Experimental setup for evaluating dissolution performance

shows the amount of total strain during powder processing to affect the dissolution performance. Shear rate did not appear to have a consistent effect on tablet dissolution performance. While increasing total strain has been correlated with increasing homogeneity using LIBS, the variability in drug release rate increases. It is currently unclear whether this is a function of content uniformity or apparatus variability.

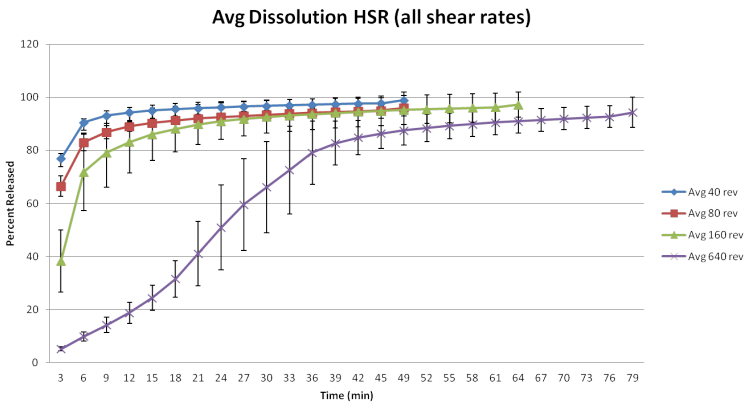

Figure 5.12: Average dissolution results for Chlorphen tablets

Solvent Penetration Analysis

The Chlorphen tablets are slightly more variable in terms of properties than the DCL tablets which were used to calibrate the method. Similar agreement can be seen in the penetration results of the low compaction force sample tablets made from Chlorphen blends as compared to the DCL tablets used to validate the experimental method. However, tablet variability appears to be more prevalent than for the mono-component tablets. Figure 5.13a shows the penetration results from the Chlorphen tablets from both blends at both compaction pressures. The results show the effect of compaction pressure on solvent penetration rate. There appear to be no real differences in the initial solvent penetration rate between the two different blends at low compaction pressures. The divergence at later time points is small, and appears to be an effect of the plateau position of the solvent penetration. While the 8kN compaction force Chlorphen tablets are of nearly identical size and density, they most likely have different microstructures which influence this plateau [7]. At the higher compaction force, the Chlorphen tablets of the two blends exhibit initially different and close-to-linear solvent penetration rates, but later have similar plateau regimes. The 640rev blend has been shown to be more hydrophobic than the 40rev blend in the works of Llusa et. al. [79]. This only appears to affect the initial rate of solvent penetration in the more compacted (14kN) tablets, while the less compacted (8kN) tablets show no appreciable effect. These results are similar to the dissolution performance of similarly processed

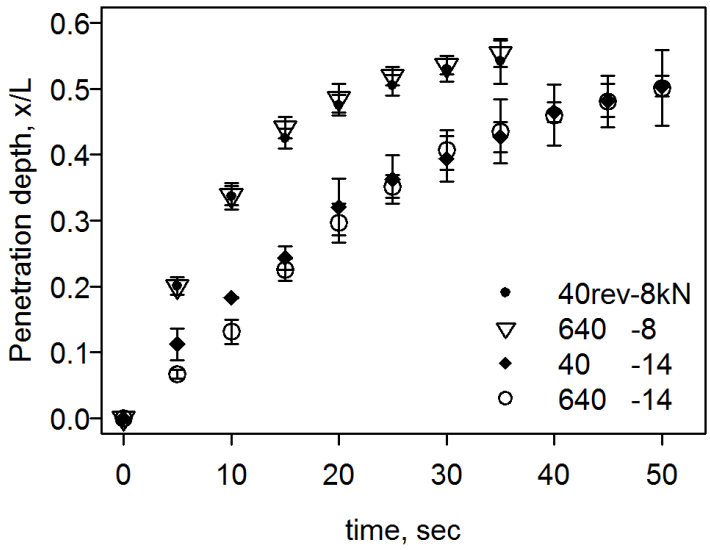

(a) Chlorphen tablets solvent penetration experimental results

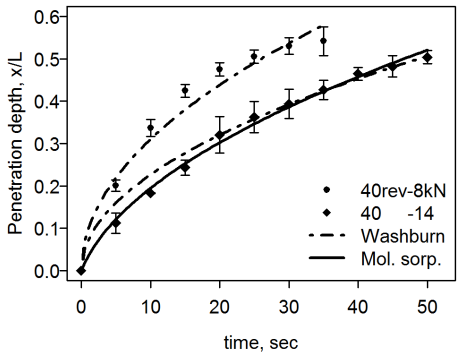

(b) Smaller total processing strain Chlorphen tablet solvent penetration modeling

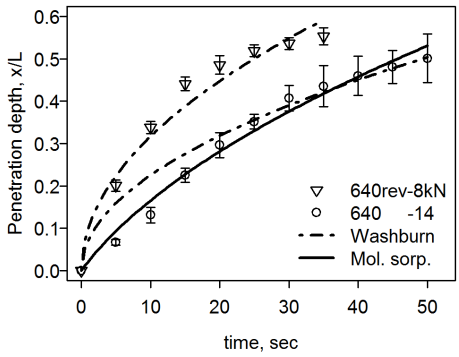

(c) Larger total processing strain Chlorphen tablet solvent penetration modeling

Figure 5.13: Experimental results and modeling of solvent penetration of Chlorphen tablets.

blends of nearly identical materials.[7] Furthermore, at the higher compaction forces, tablets made from the 640rev blend have lower tensile strength than tablets made from the 40rev blend, but allow solvent to progress through marginally slower than for tablets made from the 40rev blend. It would be assumed that the lower tensile strength tablets would be more apt to allow solvent to penetrate their matrix. As previously stated, we use the Washburn and molecular sorption models to interpret the results of our experiments. Both models are based on the capillary tube invasion idealization. The Washburn model considers penetrant motion to be determined by the balance between capillary pressure with the contact angle θ and the viscous Hagen-Poiseuille pressure

loss:

$$\frac{2\sigma cos\theta}{R} = \frac{8\mu x}{R}\mathbf{x} \tag{5.1}$$

Here x refers to the variable diffusion distance, R to the capillary radius, μ to the dynamic viscosity, σ to the surface tension. Integrating equation 5.1 with the initial condition $x(0) = 0$ leads to the well-known Washburn equation [57]:

$$x^2 = \frac{\sigma R cos\theta}{2\mu} t \tag{5.2}$$

This equation, however, fails for short times since the initial velocity $\mathbf{x} \propto 1/sqrtt$ diverges at $t \longrightarrow 0$ To fix the initial diffusion rate, Vesely [63, 64] makes an assumption that the diffusion starts at some nonzero distance B thus the modified momentum equation 5.2 becomes $\mathbf{x} = A/(x + B)$, where constant $A = \sigma R cos\theta/4\mu$ The solution of this equation with the initial condition $x(0) = 0$ gives the final expression of the molecular sorption theory:

$$x = B(\sqrt{kt + 1} - 1) \tag{5.3}$$

here $k = 2A/B^2$ is the scaling constant. Equation 5.3 accurately fits the penetration distance measurements corresponding to the Fickian, as well as Case II diffusion [63, 64]. This can be explained by a Taylor series expansion of the square root term that gives:

$$x \cong Bkt/2 \tag{5.4}$$

valid at the initial time when $kt \ll 1$. Thus, for sufficiently small values of k the penetration curve might look like a linear function on some finite time interval. For the lower compaction force tablets from both blends, it was not possible to fit the molecular sorption model to the experimental results. Figure5.13b shows the fit of the models to the solvent penetration results of tablets made from the low strain blend. At the higher compaction force, the molecular sorption model provides an acceptable fit of the data. The Washburn model fit the experimental results poorly for either compaction condition. In the case of the high compaction force tablets, the Washburn equation was

only a poor initial fit, and rectifies itself to a better fit once the solvent penetration rate begins to decay. Figure5.13c shows the fit of the models to the solvent penetration results of tablets made from the high strain blend. Neither model provides a good fit to the experimental results over the complete time interval at either compaction force. Initially, for the high compaction force tablets, the molecular sorption model more closely resembles the data, while the Washburn model is a better fit at later time points. This blend is a complex, multi-component, highly processed system, and the lack of fit to either model points to the existence of mechanisms which are not incorporated.

The results from the Chlorphen tablets show that even for the most extreme cases considered, the solvent penetration occurs at a much faster rate than the dissolution. Thus, a mechanistic model of dissolution for the tablets of these blends can be formulated in such a way that the initial conditions consider the matrix to be fully penetrated by solvent and swollen. Such an assumption thoroughly reduces the complexity of our model and reduces the parameters to be examined to 2. Furthermore, comparison of initial and final (post-swelling) tablet dimensions using the camera system will alow for better description of post-penetration porosity in the numerical model. While the solvent penetration rates may be much faster than dissolution for all cases considered, the differences in penetration rate between blends are not insignificant. These differences lend insight to changes in tablet hydrophobicity. Previous works have also focused on the relationship between blend hydrophobicity and dissolution performance[8], though changes in powder hydrophobicity are much greater than changes in solvent penetration of compacts. These changes may be representative of the degree of coating of excipient and API particles by CS and MgSt. Such a difference would most likely have a greater effect on the rate of dissolution of individual API particles as opposed to the rate at which solute diffuses from the excipient matrix or the rate at which the matrix erodes. This factor will be explored through manipulation of the dissolution rate constants of the numerical models.

In addition to the solvent penetration rate, other important data regarding tablet performance can be gleaned from these experiments. The post swelling dimensions

of the tablets are also determined. The outer dimensions of the swollen tablet are measured in two steps. The initial, dry tablet dimensions are measured using digital calipers. Using these dimensions and the final images of solvent penetration tests, the wetted dimensions are determined. The initial dry tablet and its dimensions are used to create a pixel scaling factor. By measuring the dimensions of the wetted tablet using this pixel scaling factor, the post swelled dimensions of a given portion of a tablet are determined. The volume of the swollen tablet is interpolated from these dimensions, assuming cylindrical geometry is preserved and that the swelling is consistent throughout the tablet. Using the change in dimensions of a given volume an estimation of the post penetration volume of the total tablet can be extrapolated by scaling linearly. In conjunction with this volume, the density of the particles can also be used to determine the internal porosity of the structure. The solvent penetration appears to return the tablets to a relaxed state. Analysis of the videos gives post swelling dimensions of 5.2mm radius and 7mm height. This means the post swollen volume is $595mm^3$. Using the mass based percentages and true densities of the individual components and an average tablet mass of 540mg, the predicted volume of the tablet should be $371mm^3$. This means the unoccupied space in a tablet is 38% of the total volume.

5.3 Numerical Predictions

The tablets examined in these physical experiments are emulated using numerical modeling. The models will be constructed so that their performance can be modeled using the aforementioned simulation framework. The solvent penetration experiments have already shown the rate of solvent progression through the matrix occurs much faster than drug release, so the initialization of the model will occur at a point in time when the excipient matrix is fully "wet". These dimensions are extrapolated from the solvent penetration experiments, using the post swelling images. For simplicity, it will be assumed that all volume unoccupied by solid material will contain solvent. This solvent concentration increases as solid particles dissolve, thus increasing the available volume for solvent. Drug concentration is initially uniformly distributed in the form of monosized, spherical particles. It is assumed the solute diffusion constant will be unaffected

by increased processing strain, and thus the fastest dissolving tablets will be used to determine an acceptable value to be used by all simulated tablets. The primary focus will be the change in the dissolution rate of the individual drug particles as as result of processing strain and the effect on available API surface area. Surface erosion will be considered as zero. The complete model is defined by 15 parameters, the majority of which are measured directly from the given materials, or are values supplied by the material supplier or in literature[80, 81]. The model is discretized over a 40x40x40 grid with cell dimensions of 0.296 x 0.296 x 0.199 mm. The timestep was 0.1 second.

Parameter	**Units**	**Acquisition**	**Possible Value**
Tablet thickness	mm	Measured	7.0
Tablet radius	mm	Measured	5.2
API particle radius	mm	MSDS	0.045
Lactose particle radius	mm	MSDS	0.050
API content	mg	Measured	45.1
Lactose content	mg	Measured	202.5
API density	mg/mm^3	MSDS	1.295
Lactose density	mg/mm^3	MSDS	1.500
API solubility	mg/mm^3	MSDS	0.01278
Lactose solubility	mg/mm^3	MSDS	0.0216
Solute diffusivity	mm^2/s	Tuned	0.10
API dissolution coefficient	mm^2/s	Tuned	1, 0.50, 0.25, 0.040
Lactose dissolution coefficient	mm^2/s	Tuned	1, 0.50, 0.25, 0.040
Initial porosity	normalized	Calculated	0.38

Table 5.1: Model Parameters

As many parameters in Table 5.3 as possible are determined using experimental or published data. It is our goal to keep the number of free parameters to a minimum in order to keep results as meaningful as possible. Density, solubility and particle size are taken from the MSDS of lactose and chlorpheniramine. The tablet dimensions and porosity are calculated as described in the solvent penetration section. Surface erosion is considered to be negligible in the model of this system. Physical experiments have shown this tablet system does not disintegrate or erode under the prescribed dissolution conditions, as can be seen in Figure 5.15.

The "tuned" solute diffusivity parameter is determined using data from the low shear blends. Comparison with release rates after the solid api particles have dissolved also

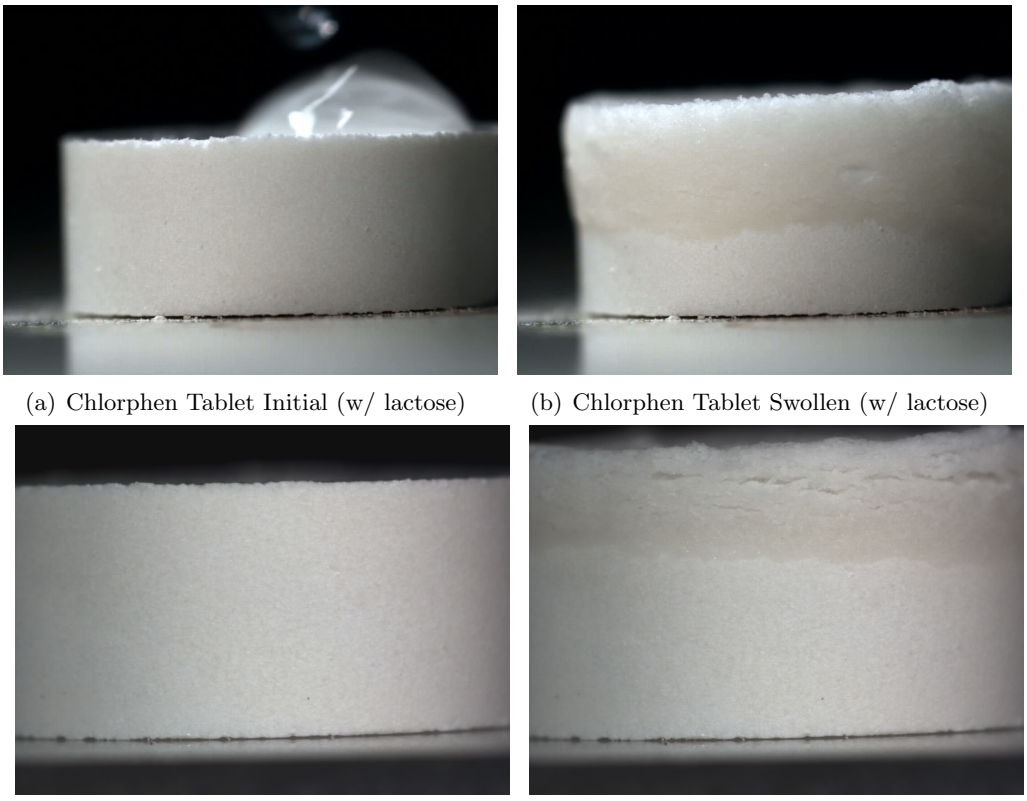

(a) Chlorphen Tablet Initial (w/ lactose) (b) Chlorphen Tablet Swollen (w/ lactose)

(c) Chlorphen Tablet Initial (no lactose) (d) Chlorphen Tablet Swollen (no lactose)

Figure 5.14: Images of swollen tablets from solvent penetration experiments.

highlights the appropriateness of the chose diffusion coefficient. As increased total strain is believed to result in the increased coating of soluble surfaces in MgSt (insoluble), tablets made from materials which have undergone less total strain have API and lactose particles with greater exposed surface area. Thus the dissolution of these tablets can be modeled through manipulation of the particle dissolution coefficient assuming solute diffusion to be generally unaffected by particle coating. Coating of particles should not change the kinetics of the solute diffusion. Changes in porosity due to the dissolution of particles are still be considered and will have some effect on solute concentration and diffusion. By determining the solute diffusion parameter which properly models the resultant dissolution performance, the performance of the remaining blends can be modeled through manipulation of the particle dissolution coefficients. Equation 4.5 shows the dependence of particulate dissolution on the available surface area, as it is included in the functional dissolution coefficient; α_C. Changing the dissolution coefficient α_{API} should have the same effect on dissolution performance as manipulating

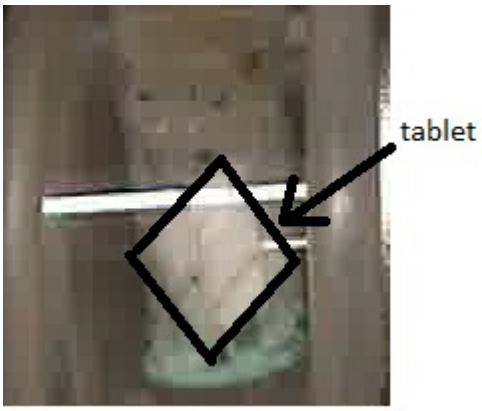

Figure 5.15: Swollen tablet in holder.

the available surface area.

5.3.1 Results of Heterogeneous Models

Using previously developed algorithms, discrete distributions of API and lactose are created. The location of the center of each particle as well as its radius is stored. The full model functions like the homogeneous version in terms of the handling of the surface, solvent and solute concentrations, but updates the solid particle properties individually. The particles in a given cell are individually described in terms of position and radius. Solvent and solute concentration are still handled on a cellular basis, and particle dissolution is calculated based on the values of the cell in which the center of each particle resides. All particles in a given cell are updated simultaneously to ensure that solubility limits are not breached. Porosity is again updated to account for decreasing solid volume fractions as particles dissolve. Figure 5.16 shows the particle size distribution histogram of active particles in the model. This distribution is based on data from the MSDS of the active component. Figure 5.17 shows the distribution of soluble particles inside a half cut of the tablet at t=0; API particles are blue and lactose particles are gold. The tablet/fluid interface, represented by the 0 level set, is shown surrounding the particles. The empty space between the particles is filled with the remaining insoluble excipients (MCC, MgSt) and solvent when the simulation begins.

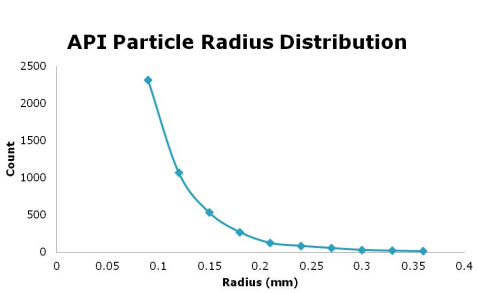

(a) Particle radius distribution

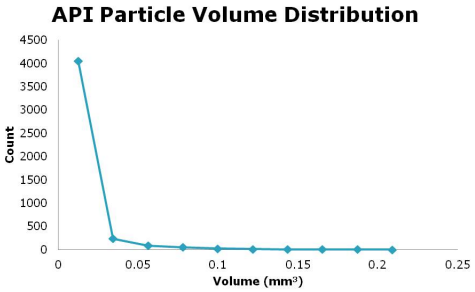

(b) Particle volume distribution

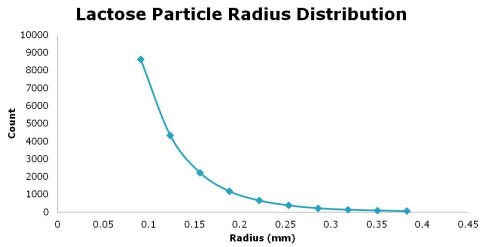

(c) Particle radius distribution

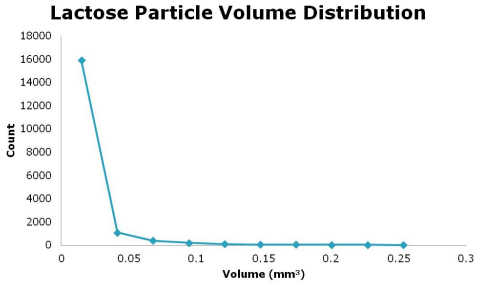

(d) Particle volume distribution

Figure 5.16: API and lactose particle size distribution of model tablets.

The effective dissolution coefficient decays exponentially as the total strain is increased as shown in Figure 5.18a. As total strain increases it is expected that the surface area available for dissolution decreases and not necessarily in a linear relationship. The decay appears exponential and seems to be reaching a limit in terms of the strain. Although further inspection of the sensitivity of the particle dissolution coefficient may show that changes in the drug release are also affected in an exponential manner by changes in the dissolution coefficient. The time to release 90% of drug from the matrix does appear to be linearly related to the total strain for the higher three total strain conditions. Figure 5.19 shows the evolution of API and lactose particles comprising the tablet matrix. The empty space between particles would be occupied by fluid or the non-dissolving components of the matrix, MCC and MgSt. Soluble particles have a decreasing surface area as they dissolve. This holds true for both the API and lactose particles. Analysis of the release profiles show very good agreement with the physical experiments for the faster dissolving tablets. Figure 5.20 shows comparisons

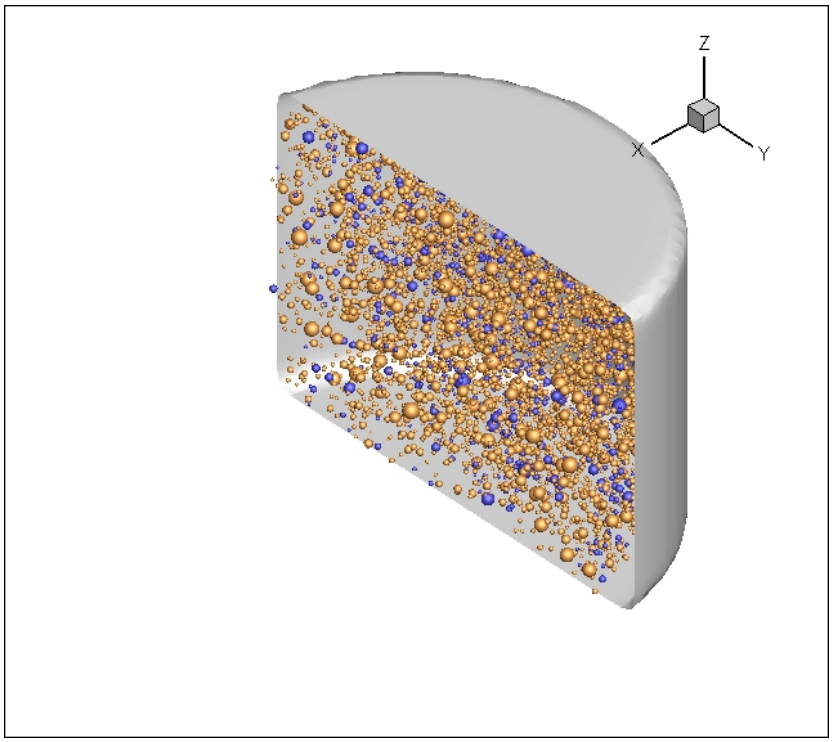

Figure 5.17: Half cut of model tablet showing API and lactose particle distribution. API particles are blue and lactose particles are gold. The particles are surrounded by the tablet/fluid interface represented by the 0 level set.

of the performance of the models and the physical tablets. As release mechanisms become increasingly complex, the model becomes unable to properly match the shape of the release curve. We believe this shape change is related to the way in which solvent penetrates the tablet matrix. For tablets made from the less processed blends, full absorption of solvent occurs more quickly than for tablets made from the most processed blend. Most likely, there are portions of the tablet which do not absorb solvent initially, closed pore structure areas, but which do absorb solvent as API and lactose particles dissolve. This would explain the shape of the release curves for the 640 rev blend tablets, which exhibit extremely slow initial release that quickly accelerates after approximately 15 minutes.

We also examined the sensitivity of the dissolution coefficient in proximity to the proposed solution values. Figure 5.21 shows the release profiles of the solution tablets as well as those with dissolution coefficients of $\pm 10\%$. The changes have the most

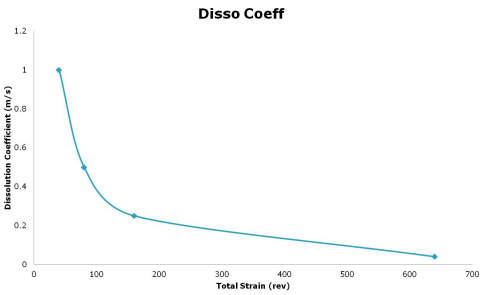

(a) Model Dissolution Coefficient vs. Total Strain

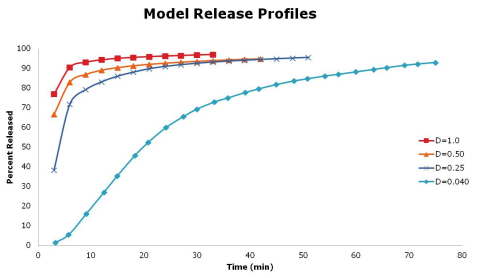

(b) Dissolution Performance of Heterogenous Models

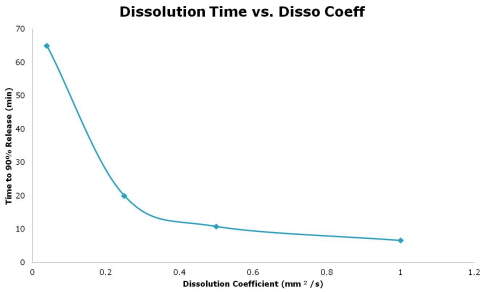

(c) Dissolution Time vs. Dissolution Coefficient

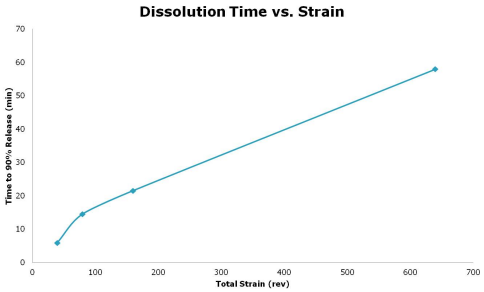

(d) Dissolution Time vs. Total Strain

Figure 5.18: Effect of dissolution coefficient on the dissolution performance of heterogeneous models. The change in total time for the tablet to reach 90% drug release is linearly proportional to the total strain on the powder blend.

effect on the release profiles of tablets with slower dissolution. The solutions of the different dissolution coefficients converge as the solid volume fraction of API reaches 0. This is because the performance becomes dominated by diffusion of the solute from the tablet matrix, for which all models have the same coefficient. The change in dissolution rates from the tablets are not linearly related to changes in the dissolution coefficient. Much smaller changes in the value for more slowly dissolving tablets is indicative of the increasing dominance of this process.

The model performs adequately for our given system. Additional considerations can be made in future iterations which incorporate the mechanisms necessary to produce the more complex systems with greater accuracy.

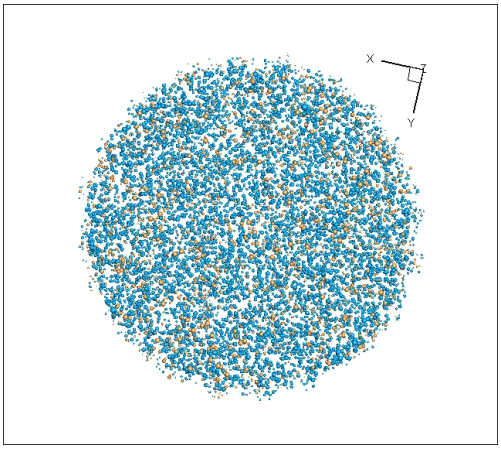

(a) Model Tablet for 40 rev Strain Tablets 50 sec

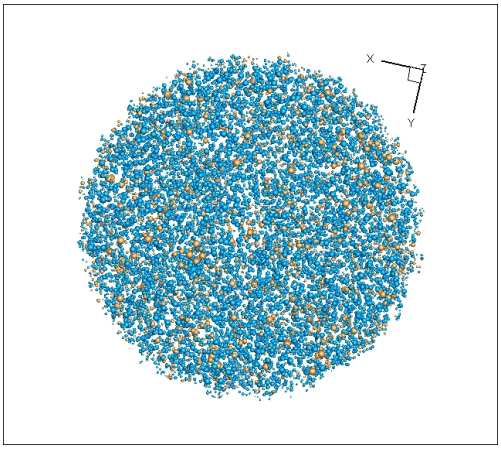

(b) Model Tablet for 80 rev Strain Tablets 50 sec

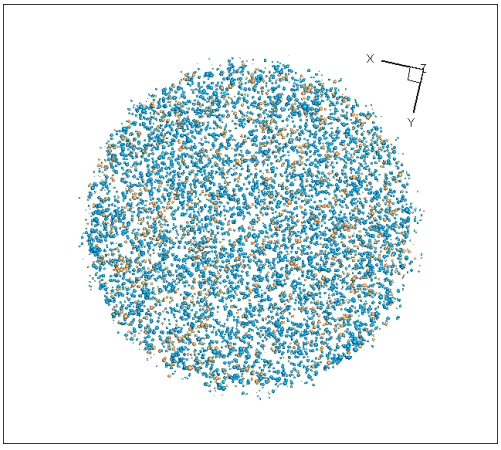

(c) 100 sec

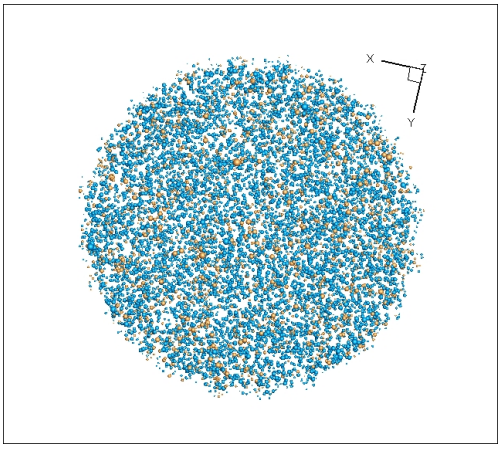

(d) 100 sec

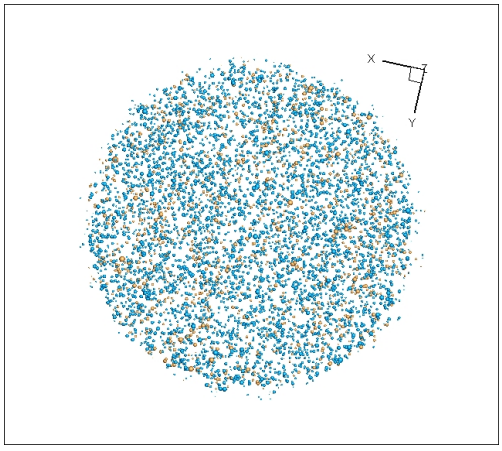

(e) 150 sec

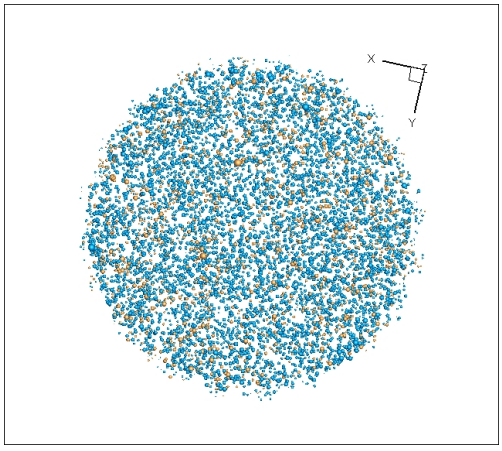

(f) 150 sec

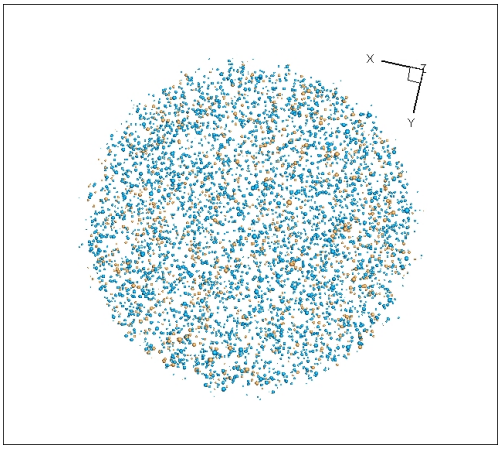

(g) 200 sec

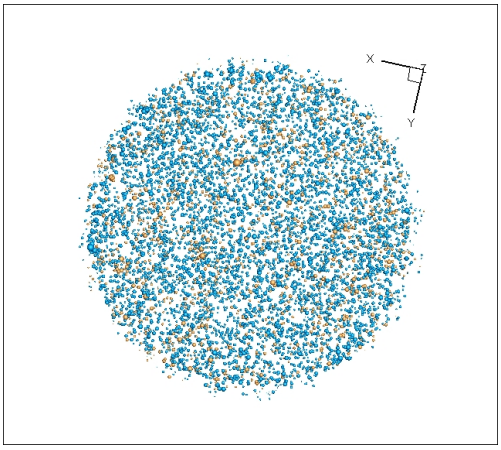

(h) 200 sec

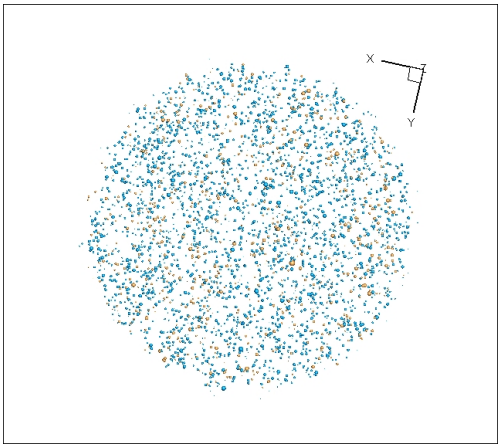

(i) 300 sec

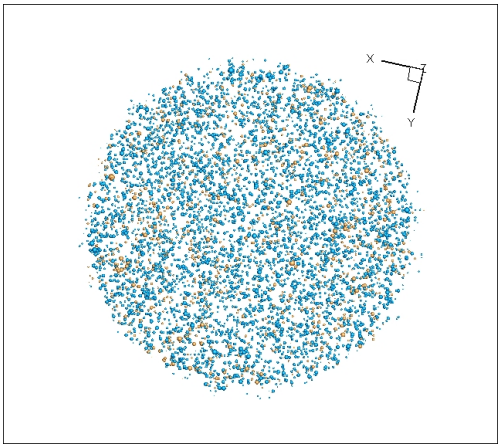

(j) 300 sec

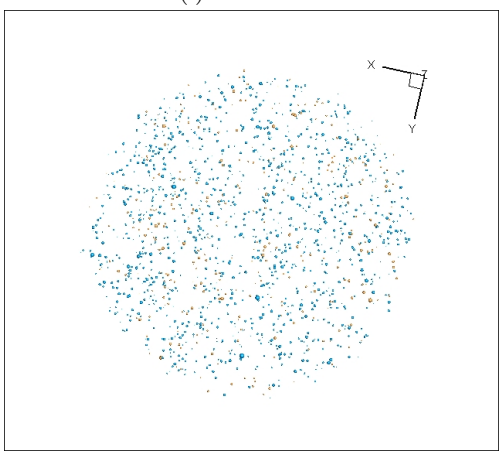

(k) 500 sec

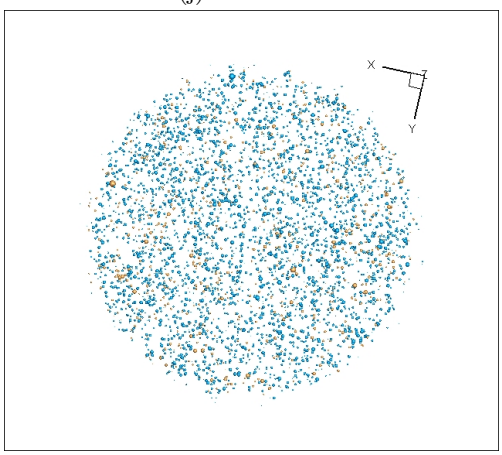

(l) 500 sec

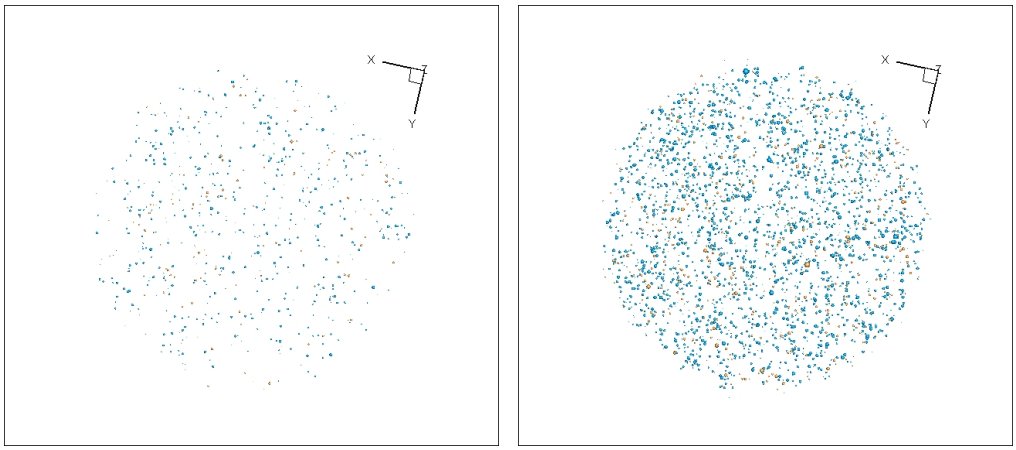

(m) 700 sec (n) 650 sec

Figure 5.19: Evolution of discrete tablet models. API particles are blue and lactose particles are gold.

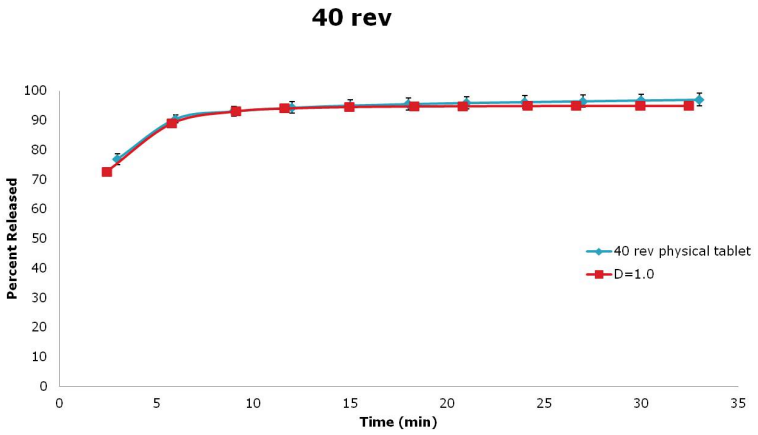

(a) Model Tablet for 40 rev Strain

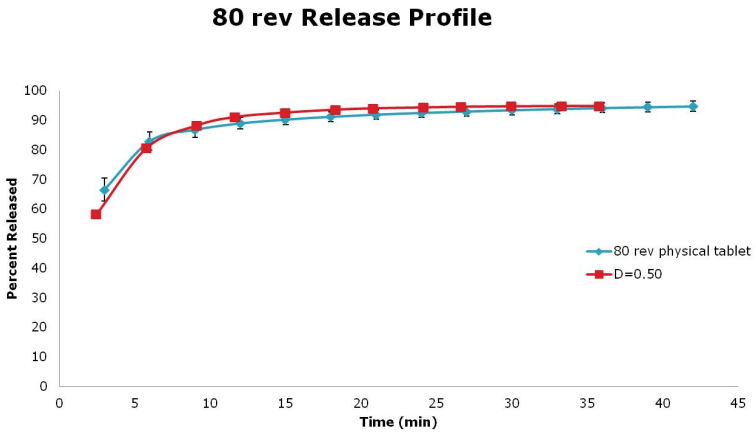

(b) Model Tablet for 80 rev Strain

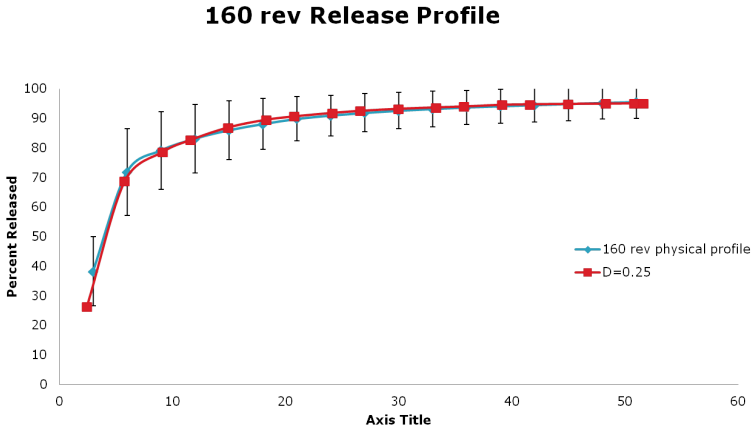

(c) Model Tablet for 160 rev Strain

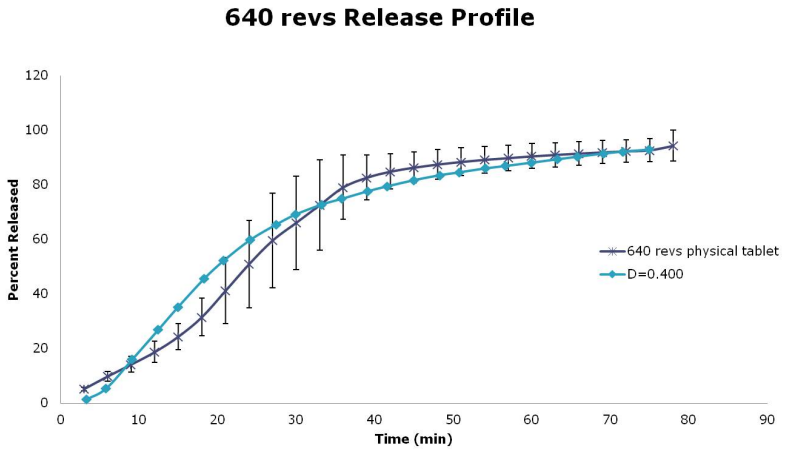

(d) Model Tablet for 640 rev Strain

Figure 5.20: Physical release profiles compared to discrete models

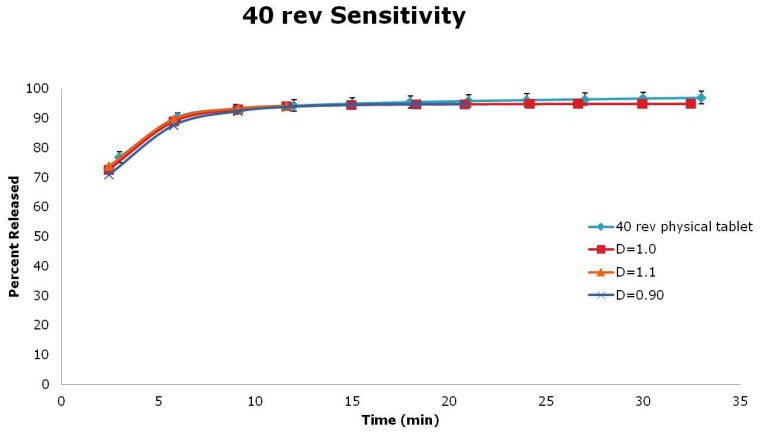

(a) 40 rev Strain

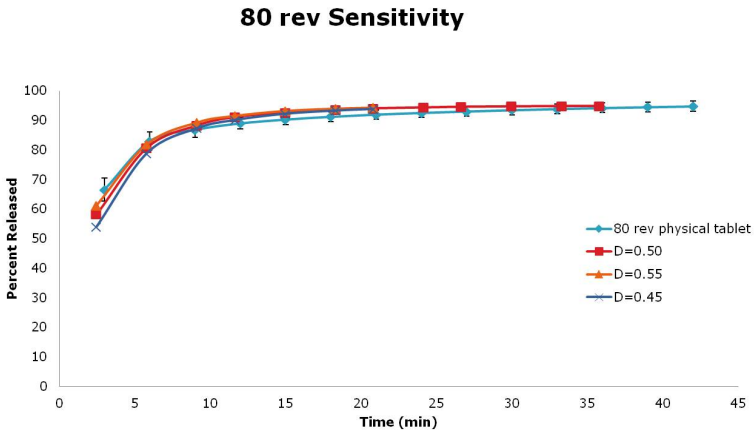

(b) 80 rev Strain

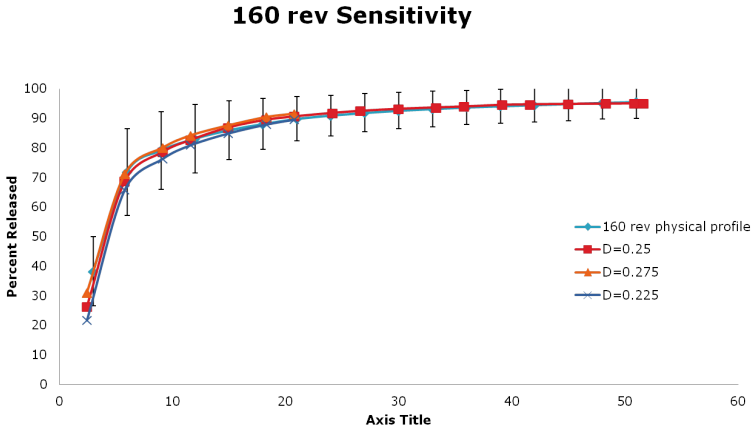

(c) 160 rev Strain

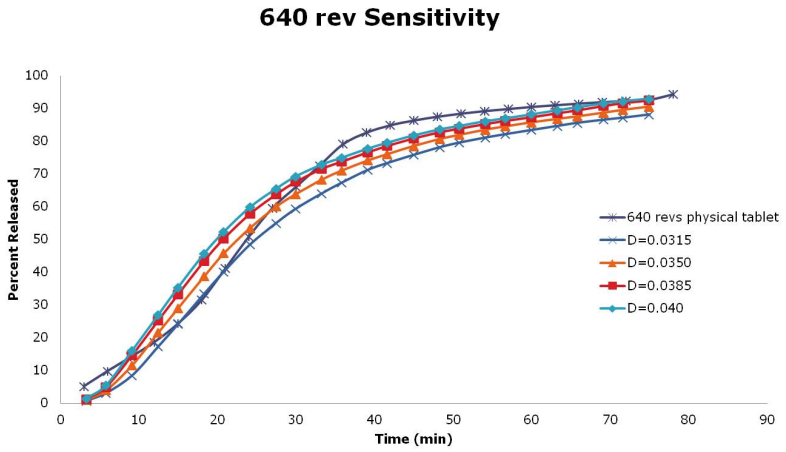

(d) 640 rev Strain

Figure 5.21: Sensitivity of release to particle dissolution coefficient

Chapter 6

Solid Oral Dosage Form with Erosion Dominated Drug Release

6.1 Introduction

The tablets analyzed in this section were created using granulations of gabapentin. The granulations were created as part of a NIPTE investigational project on the effects of granulation and compaction parameters on product performance.

6.2 Experimental

6.2.1 Base Materials

All of the different blends were made to study the effects of processing conditions and were based on the same material recipe shown in Table 6.1.

Addition Point	**Material**	$\%w/w$	**Charge Mass (g)**
Intragranular	Gabapentin	67.49	937.5
Intragranular	Klucel EF	4.5	62.5
Extragranular	Avicel PH 102	11.25	156.27
Extragranular	Starch	6.75	93.76
Extragranular	Klucel EXF	4.5	62.51
Extragranular	Crospovidone	2.47	34.31
Extragranular	Poloxamer	1.24	17.22
Extragranular	Talc	1.01	14.03
Extragranular	MgSt	0.79	10.97

Table 6.1: Blend Composition

Batch	Water Content(g)	Wet Massing Time (s)	Granulation Time (s)	Total Process Time (s)	Spray Rate (g/min)	Impeller Speed (rpm)
96251-2	50	30	105	135	28.5	420
96251-3	30	30	63	93	28.5	420
96251-4	40	30	84	114	28.5	420
96251-5	40	30	84	114	28.5	345
96251-6	40	30	10	40	249.6	345
96251-7	40	30	10	40	246.6	420
96251-8	50	60	105	165	28.5	420
96251-9	50	0	105	105	28.5	420
96251-10	50	30	105	135	28.5	420
96251-11	50	30	105	135	28.5	420
96251-12	50	30	105	135	28.5	420
96251-13	50	30	105	135	28.5	420
96251-14	50	30	105	135	28.5	420
96251-15	50	30	105	135	28.5	420

Table 6.2: Granulation Parameters

6.2.2 Manufacture

Several blends were granulated using the following procedure. Intragranular material is charged into GEA Collette UltimaGral 10L granulator as shown in Figure 6.1a. This is a top-down Diosna impeller configuration model. The components were first dry blended in the granulator for 5 minutes with an impeller speed of 420 rpm. Granulation was then performed using the settings in Table 6.2:

After granulation, the wet mass was transferred to a GPCG1, Figure 6.1b, and dried as specified in Table 6.3. The dried material was weighed and then charged into a Servolift 5L bin blender, Figure 6.1c, along with the remaining extragranular material, mass adjusted to correspond to the initial batch percentages. The blender was rotated at 15rpm for 2.5min.

Tablet Compaction

The resultant blends are then compacted into tablets using a Presster®tablet press simulator. The Presster®is set to simulate a Manesty BB4 35 station press, making

Batch	Total Drying Time (s)	Max Outlet Temp ($\deg C$)	LOD (%)
96251-2	1000	20	1.13
96251-3	1000	21	0.89
96251-4	1000	21	1.06
96251-5	1000	21	1.03
96251-6	1000	21	0.83
96251-7	1000	21	1
96251-8	1000	21	1.19
96251-9	1000	21	1.16
96251-10	2500	37	0.21
96251-11	1500	30	0.6
96251-12	500	25	1.49
96251-13	1000	23	1.17
96251-14	1000	21	1.27
96251-15	1000	21	1.18

Table 6.3: Drying Parameters

tablets at a rate of 150000 per hour, or 25rpm, using a set of 17.5mm concave elliptical punches made of S7 steel. The punches were designed to make tablets like those depicted in Figure 6.2. Compaction is controlled to produce tablets at predetermined compression forces; 10, 15 and 20kN. As this is not a direct setting, the compression and dosing heights are adjusted specifically for each processed batch, and any tablets whose density falls outside the prescribed range is discarded immediately. Tablet target mass is within a tolerance of $\pm$15mg, and target compaction force is within $\pm$ 1.0kN.

6.2.3 Characterization

Acceptable tablets are then subjected to one of two tests; breaking force/hardness test or erosion testing.

Tablet Hardness

Tablet hardness is measured using a Dr. Schleuniger Pharmatron 6D tablet tester. Tablets are placed in the tester so that they are broken along the minor axis of the oval cross section. Hardness of tablets from Blend 12 compressed at 15kN is 10.4 kP

(a) Granulator

(b) Dryer

(c) Blender

Figure 6.1: The images above show the equipment used to process the gabapentin granulations before compaction.

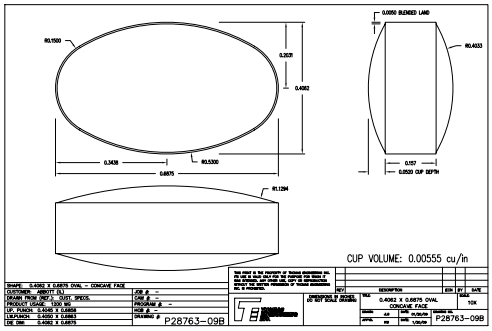

(a) Ideal Tablet Dimensions

(b) Oval Punches Used for Compaction

Figure 6.2: Ideal tablet dimensions and oval punch used for compaction.

±0.3kP.

Solvent Penetration Analysis

As with the previous tablets, it is important to understand how fluid penetrates the tablet matrix. The penetration of solvent in the matrix causes changes in the matrix composition. It begins the process by which the cohesive bonds between particles are reduced and changes the likelihood of a segment of tablet eroding. In order to determine the basic solvent penetration profile, several tests are performed using a small dish of stagnant DI water. The tests consist of 4 steps: First, the dry tablet dimensions are measured using Mitutoyo digital calipers,. The measurements are taken using minimal pressure with the tips of the caliper jaws. Then the tablet is placed in the DI water for a predetermined length of time. Either 1 or 2 minutes. The tablet is then removed

Batch	Compaction Force (kN)	Time (s)	Erosion Depth (mm)	Gel Thickness (mm)
96251-2	10	60	0.60	0.27
96251-2	15	60	0.30	0.19
96251-2	20	60	0.17	0.07
96251-2	10	120	0.81	0.46
96251-2	15	120	0.38	0.20
96251-2	20	120	0.27	0.16
96251-3	10	60	1.05	0.45
96251-3	15	60	1.02	0.20
96251-3	20	60	0.71	0.07
96251-3	10	120	1.49	0.53
96251-3	15	120	1.21	0.38
96251-3	20	120	0.87	0.19
96251-12	10	240	0.91	0.35
96251-12	15	240	0.53	0.14
96251-12	20	240	0.22	0.10

Table 6.4: Tablet erosion in stagnant DI water.

from the media, and the dimensions are again measured using digital calipers. This time special handling is required so as not to damage the wetted tablet. One set of measurements represent the dimension of the tablet including the gel layer at the surface. The tablets are then measured using increased pressure to find the dimensions of the solid portion. The tablet is then cut in half along its minor axis and the cross sectional face imaged. The location and thickness of the gel layer in time are important in characterizing the way in which solvent penetrates the tablet matrix. The results of these experiments are displayed in Table 6.4. The results indicate there are differences in solvent uptake and disintegration due to both processing conditions and compaction. The sharp solvent front, visible in Figure 6.3, is indicative of Case II diffusion. Unlike the smooth profile achieved by Case I or Fick's diffusion, the solvent profile inside the tablet is practically discontinuous with completely dry sections remaining inside the tablet.

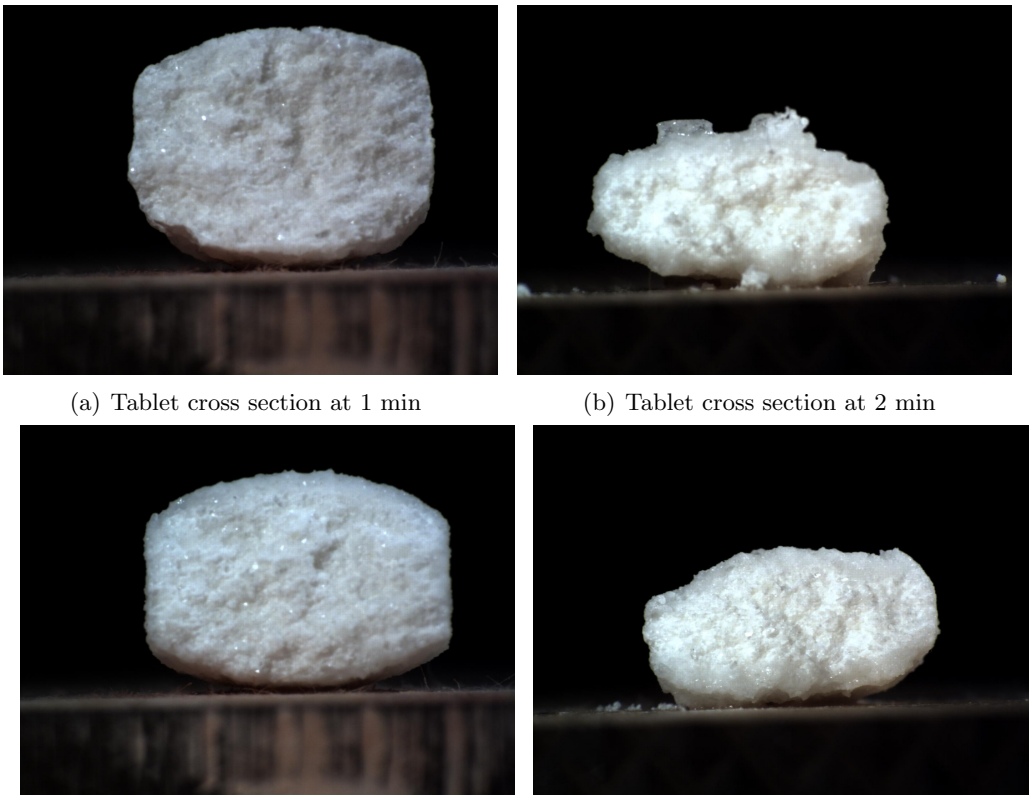

(a) Tablet cross section at 1 min (b) Tablet cross section at 2 min

(c) Tablet cross section at 1 min (d) Tablet cross section at 2 min

Figure 6.3: Images of the gel layer which forms during solvent penetration of the gabapentin tablets.

Tablet Erosion Analysis

Tablet erosion analysis is performed using equipment similar to that used for the solvent penetration tests for the tablets made from the chlorpheniramine powder blends as shown in Figure 6.4 The tablet being tested is placed in the mesh holder inside the beaker. Also inside the beaker is a magnetic stir bar set to the desired stir rate. The camera is set to record, then 200mL of distilled water at 37.5°C is poured into the beaker, which is set atop a preheated hotplate. The images are processed by hand using a three step process. First, the starting point on the videos is syncronized based on the moment the last of the fluid media is poured into the erosion vessel. Then the videos are used to produce an image every 10-20 seconds using avidemux 2.5 (available online: http://avidemux.berlios.de/). These images are then opened using ImageJ (available online: http://rsbweb.nih.gov/ij/) and the area of the tablet is measured using the free form selection measurement tool. The resulting changes in tablet volume are shown in

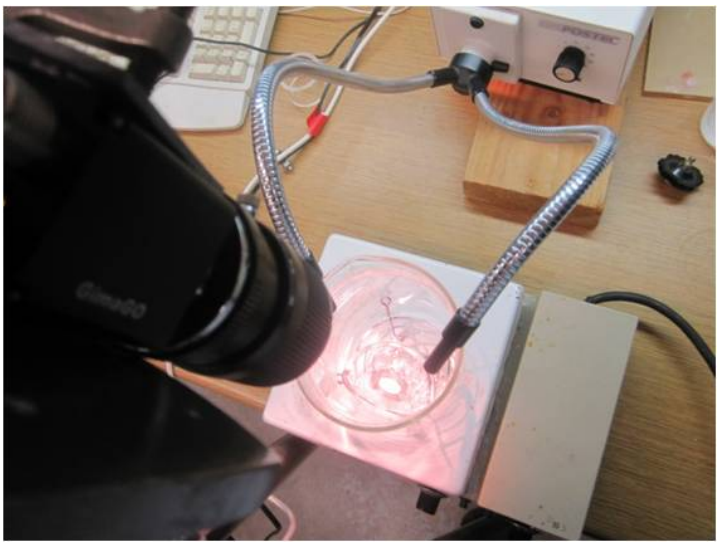

Figure 6.4: Experimental setup involved in the initial erosion analysis.

Figure 6.5. The changes are initially linear with different compaction forces exhibiting different rates of erosion. Fluid shear also has an effect on erosion rate, though this effect is more pronounced for tablet compacted at lower forces.

First a 0.01inch hole is drilled in the center of the top oval shaped surface of the tablet. A bent metal rod is then dipped in hot glue and inserted into the tablet hole. The tablet is then suspended inside a dry beaker with a magnetic stir bar atop a magnetic stirring hotplate. Once both cameras have begun recording, 200mL of distilled water at 37.5°C is poured into the beaker, though not directly on top of the tablet. Figure 6.6c and d show sample images collected during erosion experiments performed using this setup. The images are processed by hand using a three step process. First, the starting point on the videos is syncronized based on the moment the last of the fluid media is poured into the erosion vessel. Then the videos are used to produce an image every 10-20 seconds using avidemux 2.5 (available online: http://avidemux.berlios.de/). These images are then opened using ImageJ (available online: http://rsbweb.nih.gov/ij/) and the area of the tablet is measured using the free form selection measurement tool. The resulting area profiles shown in Figure 6.7 are examined to better understand the erosion processes. As the speed settings for the stir bar are of a simplistic nature, the actual flow rate of the fluid was also estimated using image analysis. Sets of images from each

Speed Setting	1	2	3
Fluid Velocity (m/s)	0.058	0.115	0.230
Reynolds	2.9	5.75	11.5

Table 6.5: Reynolds numbers of flows.

experiment are collected, and the positions of moving particles are tracked between frames. The change in position is used to calculate the velocity of the particles which is assumed to be the velocity of the bulk fluid. The velocities are used to calculate the effective Reynolds numbers of the flows as displayed in Table 6.5. Previous works on tablet erosion [82] claim Reynolds number of flows a tablet will experience during the disintegration process range from .01 to 30. The Reynolds numbers for flows used in our experiments fall within those values.

6.3 Numerical Modeling

Previous experiments with these tablets have involved the use of dissolution and disintegration assays. Results from the dissolution experiments, while unfortunately of low resolution, show the percent drug release at 10 minutes is well correlated with the average disintegration time of other tablets from the same blend and compaction conditions. As such, the mechanism governing drug release in the models will be disintegration at the surface. The erosion of a given tablet will be coupled with the solvent penetration of the tablet matrix. The results of the erosion experiments provide target erosion profiles. This includes the measured erosion rate and its dependence on tablet density/tensile strength as well as the flow of the surrounding fluid and the wetted gel layer thickness. This information combined with the measured external dimensions, mass, assumed material composition and properties of these materials should allow for meaningful determination of the governing parameters and highlight differences in material performance as a result of processing parameters. Numerical efforts focus on tablets from Blend 12 since the most detailed experimental data is available for this

batch. The governing mechanisms of release are erosion influenced by the surrounding shear field and internal solvent concentration. The solvent penetration experiments show the penetration to be very close to Case II. From this basis we assume the rate of solvent penetration to be hyperbolic and that it will decay quickly as the distance from the solid fluid interface increases. As the internal solvent concentration increases, the integrity of the matrix will weaken. This will in turn make the matrix more susceptible to shear erosion. Thus we seek to couple the effects of solvent concentration, surface shear and erosion. The initial models are defined in terms of the framework described in the model generation section. The location of the surface is represented using a level set, and all nodes lying inside the surface are assigned cell based values for solvent concentration, active content, porosity and diffusivity. As the solvent penetration mechanism greatly diverges from Fickian diffusion, the solvent penetration will be computed based on the distance from the tablet/fluid interface. The exact formulation will be described in the following section. Once solvent penetrates the surface, the internal active particles exposed to solvent will begin to dissolve, changing the internal porosity. The solvent concentration will be used to determine the movement of the surface. As the local solvent concentration reaches a critical value, which depends on the shear environment, the surface is eroded and the level set updated to account for this.

6.3.1 Solvent Penetration

Solvent penetration of the tablet matrix is the driving factor for disintegration of the gabapentin tablets. Our erosion experiments have shown the erosion rate to be approximately linear even in a stagnant fluid environment. Analysis of the gel layer thickness indicates Case II type solvent penetration. To model this a hyperbolic function has been chosen to represent the rate of solvent penetration.

$$\frac{\partial C_{sv}}{\partial t} = v_{sv} sech(x - v_{sv} t) \tag{6.1}$$

Where:

C_{sv}=concentration of solvent.

t=time in seconds.

v_{sv}=velocity of solvent front.

x=distance from bulk fluid interface.

Figure 6.8 shows the shape of the solvent penetration velocity. It is not as abrupt as a heaviside function, as the solvent concentration does have a slight gradient. When coupled with a moving surface, this function should result in a linearly moving solvent front and fairly steady gel layer thickness.

6.3.2 Moving Surfaces

Surface erosion is influenced by the local solvent concentration. As the solvent concentration increases, so does the rate at which the surface moves.

$$F = -v_{sv} * C_{sv} \tag{6.2}$$

Where:

F=velocity of the surface.

C_{sv}=concentration of solvent.

v_{sv}=velocity of solvent front.

Equation 6.2 handles the calculation of the surface velocity. This velocity is used to update the evolution of the interface.

6.3.3 Results

Figure 6.9 shows the fit of the models to the experimental results. The erosion based models were able to capture the movement of the interface in part. Agreement with models was close for the initial portion of the erosion process, but deviate once the erosion rate accelerates. Analysis of the experimental results show the tablet area initially increases, indicating the tablet matrix swells as solvent is absorbed. Swelling

of tablets is also visually observed as the experiments are being performed. The model does not consider swelling, and instead relies on reducing the tablet volume proportional to the local solvent concentration. While this approach does result in the formation of a "gel" layer in the model, as indicated in the images representing local solvent concentration in the tablet matrix shown in Figure 6.10, the physical reality is slightly different. The difference in erosion rates for the top and side view areas indicates erosion is directionally preferential. The faster erosion rates associated with the side view areas indicates erosion is faster along the axis of compression. This coincides with the physical solvent penetration experiments where axial swelling was much greater than radial swelling.

Differences in the erosion rate of surfaces were visible in the physical experiments and indicate preferential erosion along the axis of compaction. Across the set of parameters utilized, the fluid flow did not result in a measurable change in basic tablet geometry, and tablets remained a similar shape throughout the course of disintegration until the final stage. While one tablet did exhibit a geometrical change, this change was the opposite of what would be expected if caused by increased fluid shear. Visual inspection of this special case indicated that the change was most likely the result of tablet microstructure as the change occurred rapidly with a few large chunks of material eroding over a short time frame. Unfortunately the model results diverge from the experimental results at later timepoints. This is especially the case for the higher shear experiments. There is most likely some unaccounted for mechanism or process which causes the accelerated erosion at later times. It is possible the drilling of a hole into the center of the tablet weakened the tablet structure near the support rod, or even allowed fluid to enter the central area of the tablets.

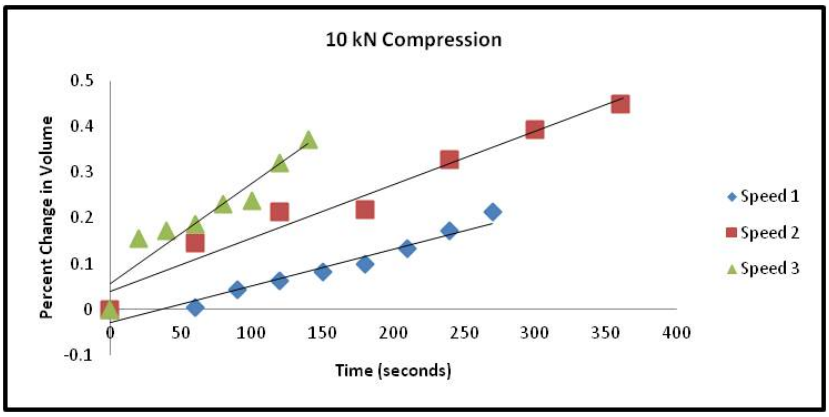

(a) 10kN Compaction Force Tablets

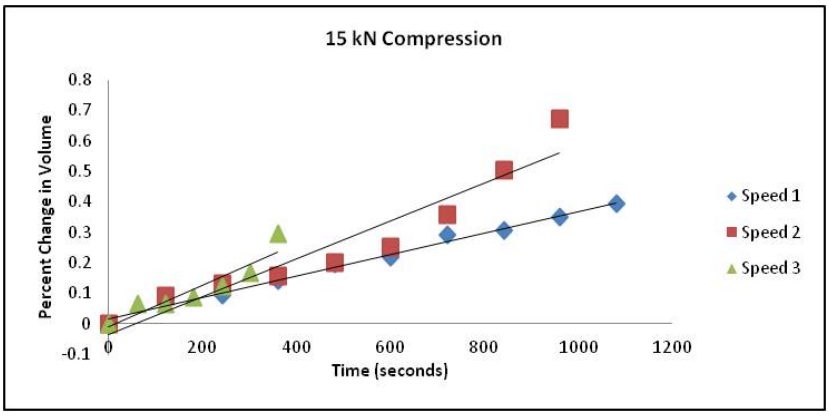

(b) 15kN Compaction Force Tablets

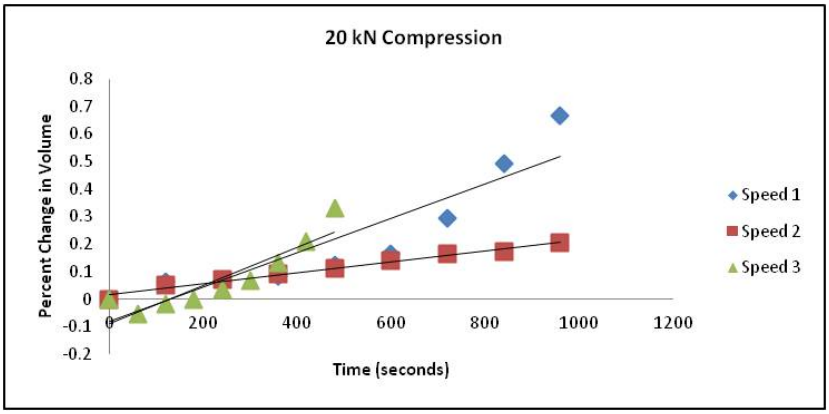

(c) 20kN Compaction Force Tablets

Figure 6.5: Results of single camera erosion experiments.

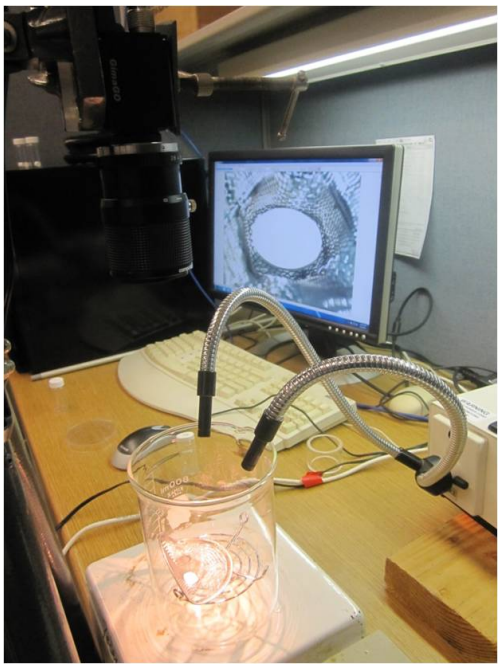

(a) Camera and Lighting Setup

(b) Sony Handicam (side view camera)

(c) Top camera (GimaGo) image

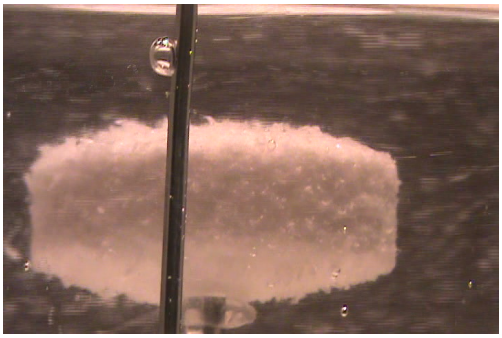

(d) Side camera (Handicam) image

Figure 6.6: Components involved in the two camera erosion analysis.

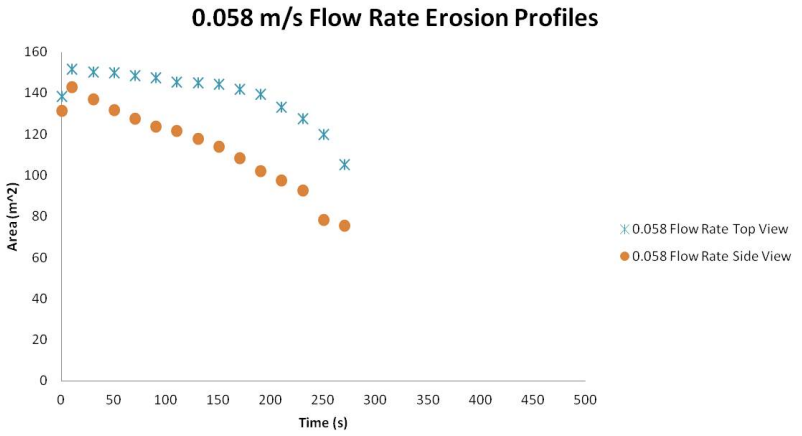

(a) 0.058 m/s Flow Rate

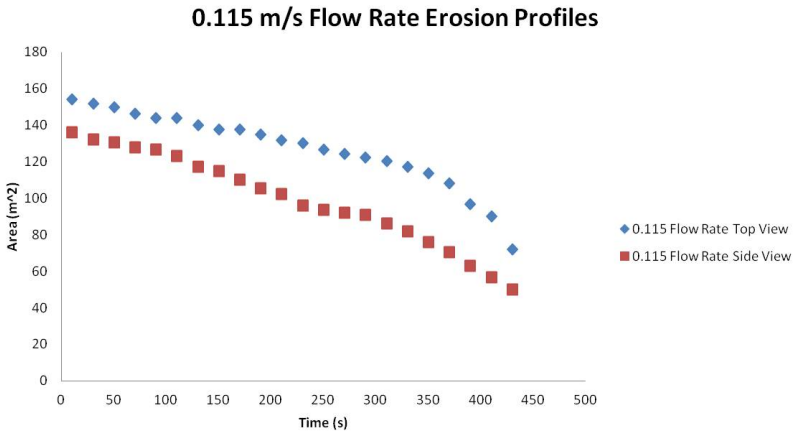

(b) 0.115 m/s Flow Rate

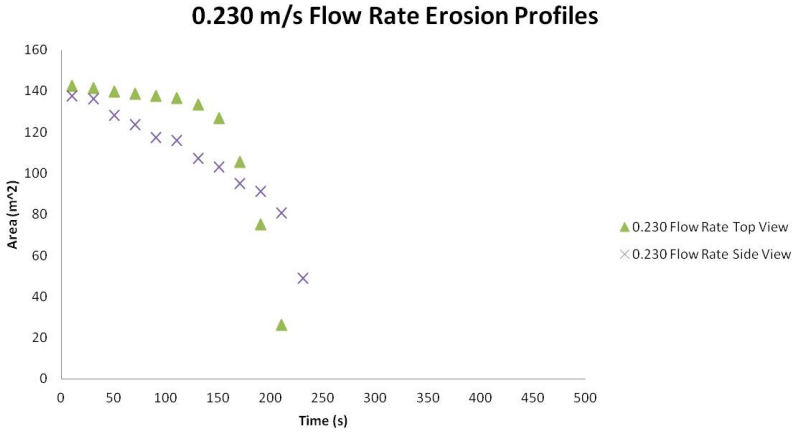

(c) 0.230 m/s Flow Rate

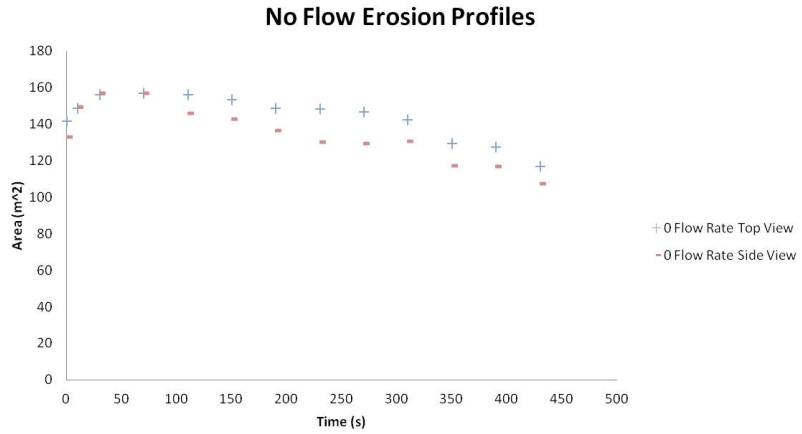

(d) 0 m/s Flow Rate

Figure 6.7: Results of two camera physical erosion experiments.

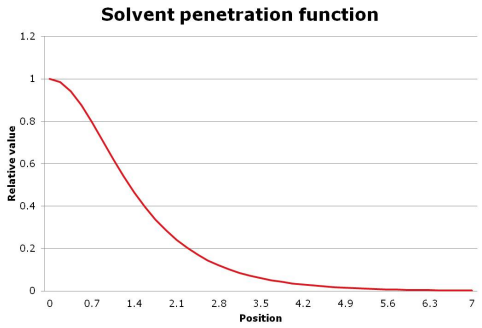

Figure 6.8: This curve represents the shape of the solvent penetration function. As the distance from the tablet/fluid interface increases so does the penetration velocity. This focuses the the solvent penetration near the surface of the tablet forming in the gel layer.

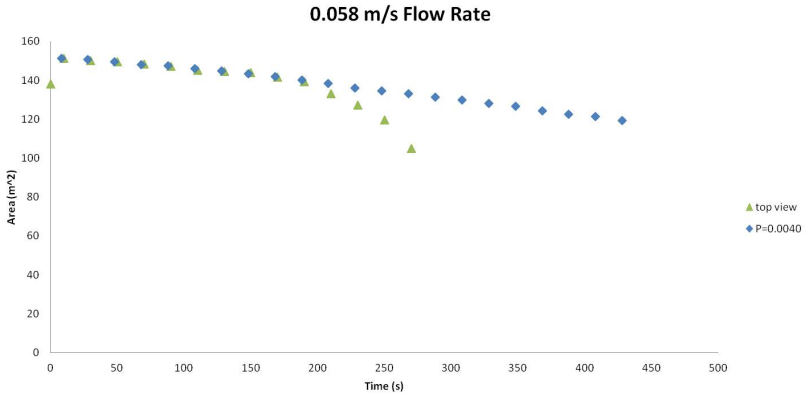

(a) Slow Stirred Erosion Top

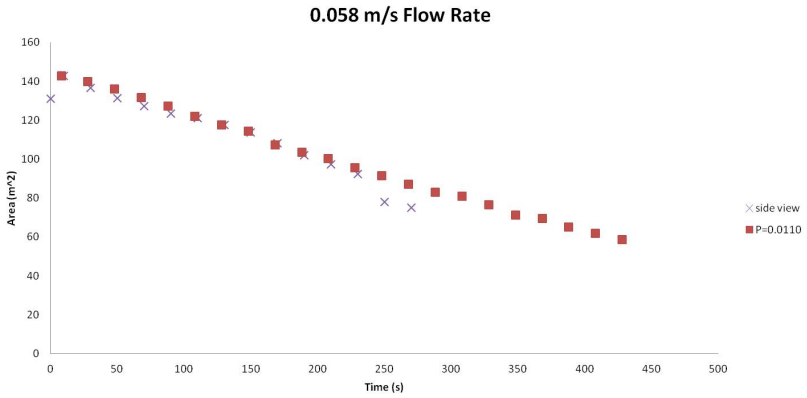

(b) Slow Stirred Erosion Side

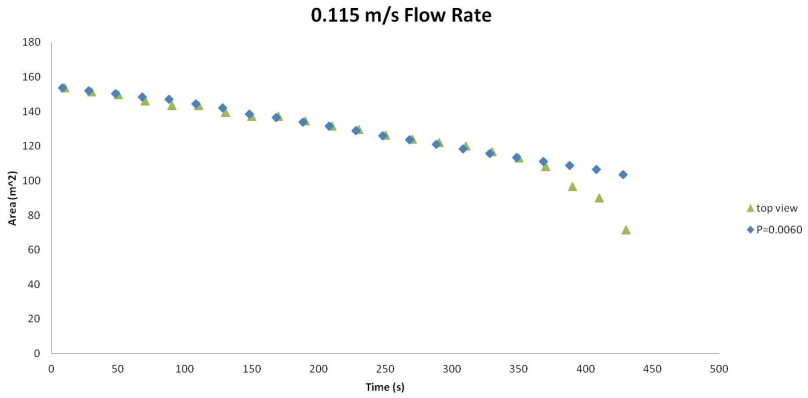

(c) Medium Stirred Erosion Top

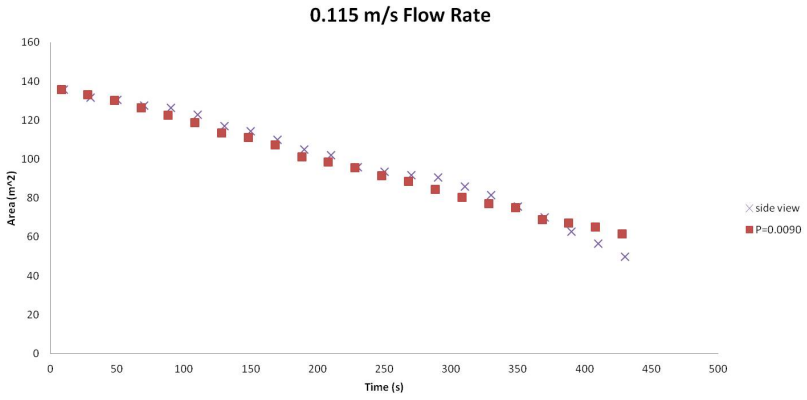

(d) Medium Stirred Erosion Side

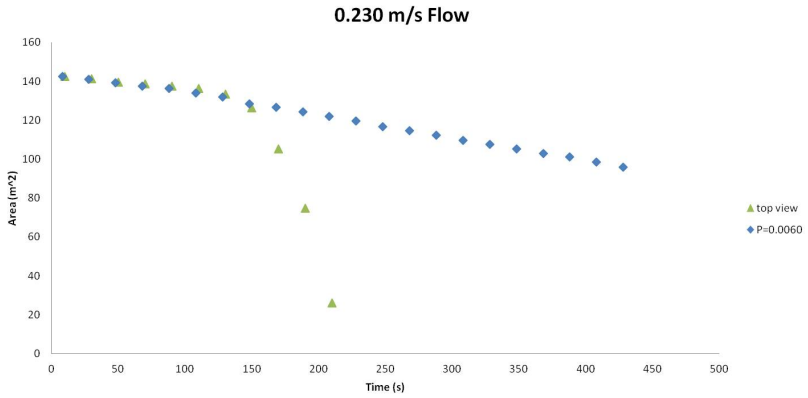

(e) Fast Stirred Erosion Top

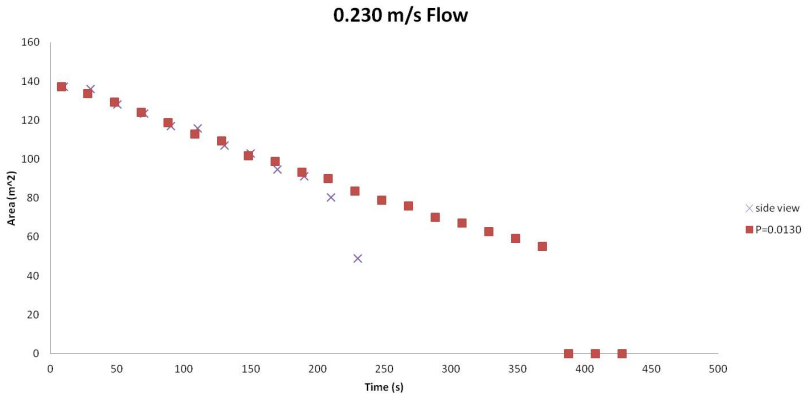

(f) Fast Stirred Erosion Side

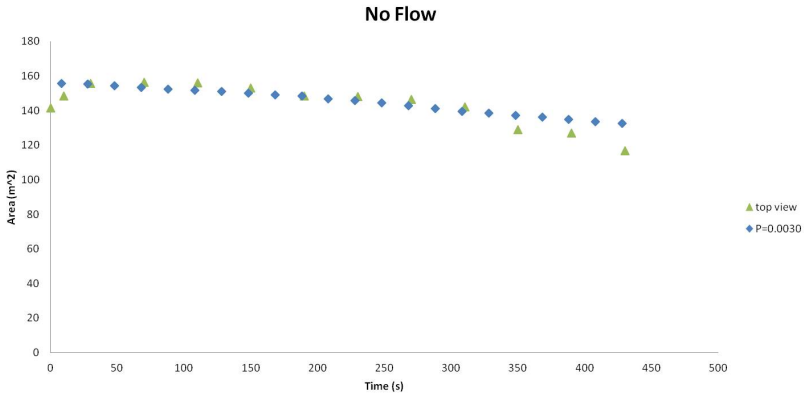

(g) Stagnant Erosion Top

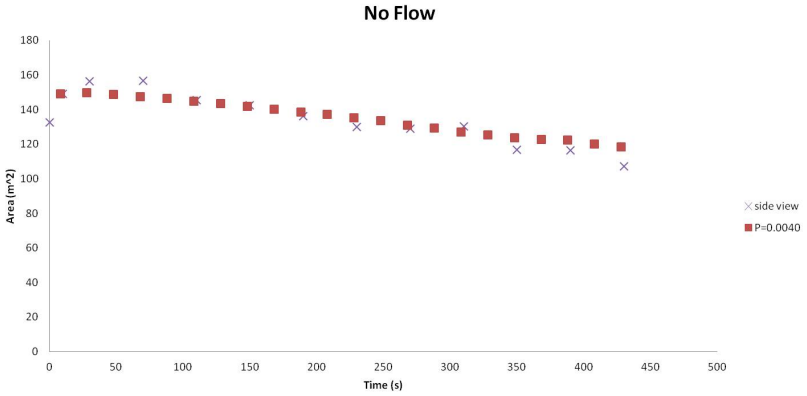

(h) Stagnant Erosion Side

Figure 6.9: Erosion simulation results.

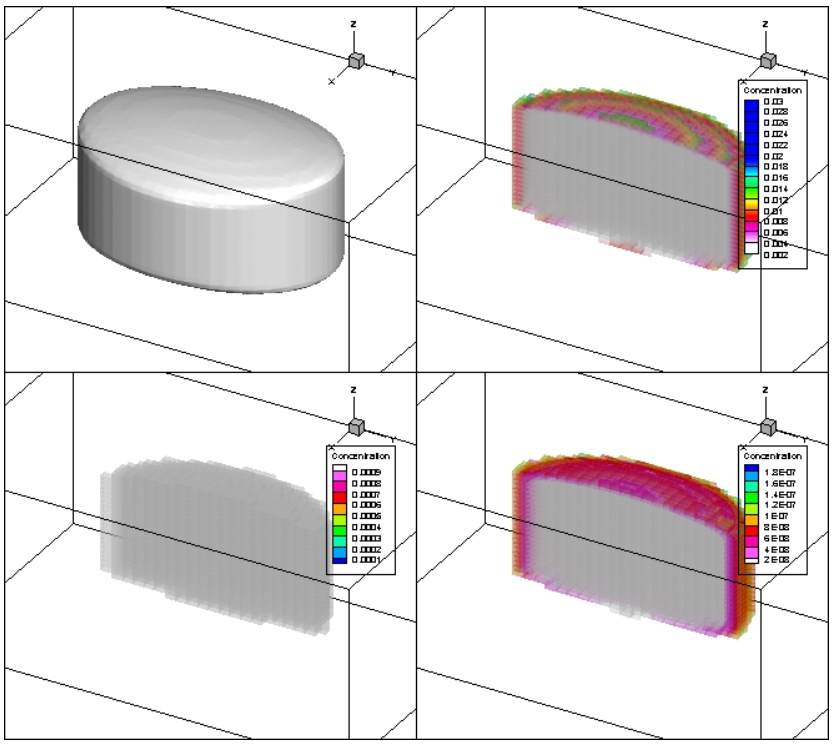

(a) Time=50s

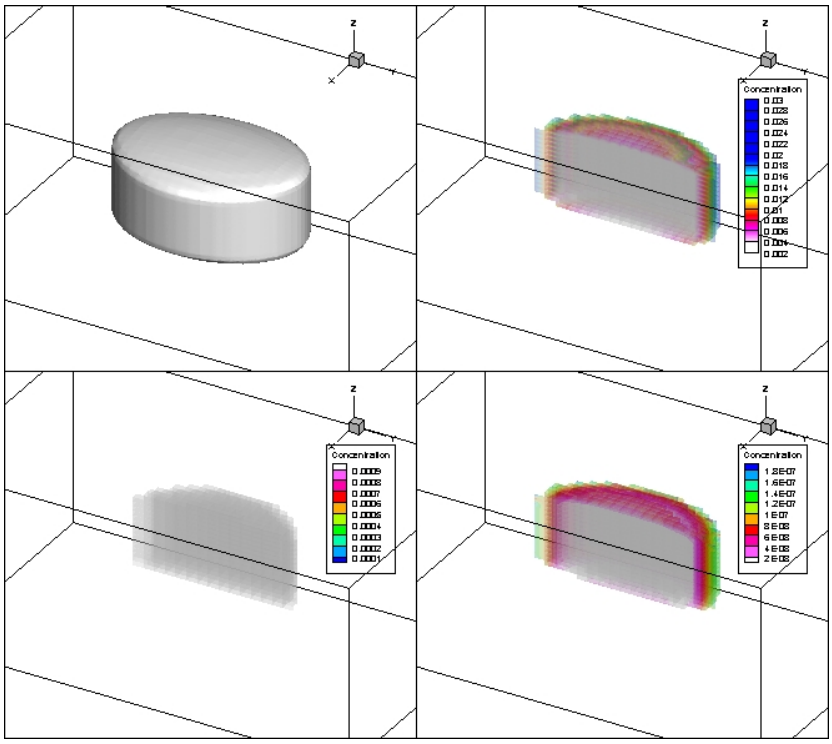

(b) Time=100s

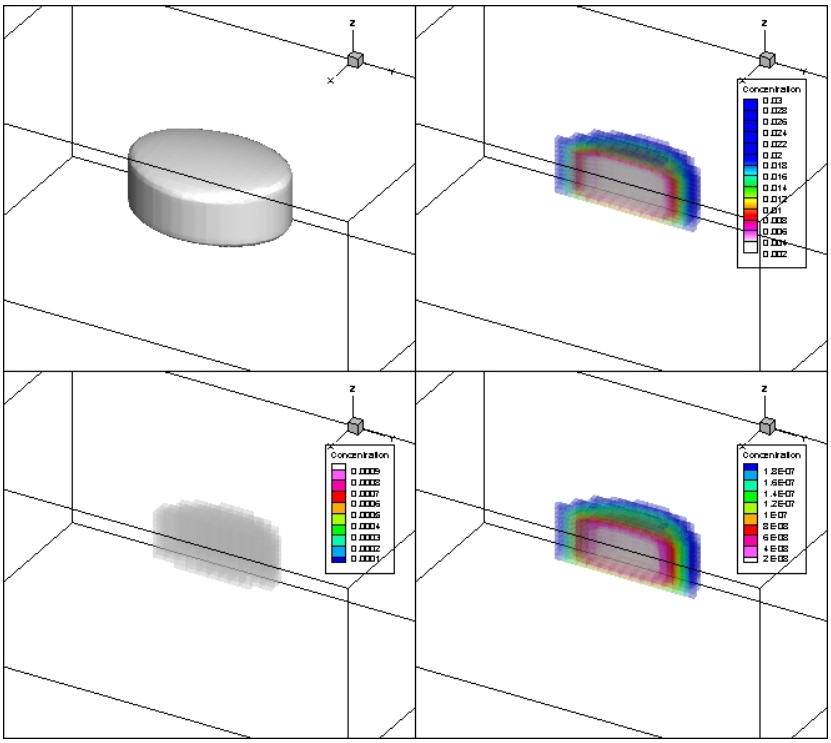

(c) Time=200s

Figure 6.10: Erosion Model Evolution. Panels clockwise from top left represent: location of tablet/fluid interface, solvent concentration, solute concentration, solid active concentration

Chapter 7

Conclusions and Future Work

7.1 Conclusions

This dissertation focuses on the development of a combined modeling and experimental approach for characterizing and quantifying the drug release performance of compacted solids, such as pharmaceutical tablets, attending to material properties and processing variables. In order to properly define the models and governing mechanisms of action, several new experimental assays were developed. These assays produced the necessary data to complete the modeling herein, and remain useful tools for further exploration of additional systems. Two representative pharmaceutical formulations have been selected in this study: one where drug release is dominated by diffusion and another by erosion. The main findings/conclusions/contributions of this dissertation can be grouped as:

1. Development of protocols for spatial characterization of tablets using Laser-Induced Breakdown Spectroscopy (LIBS) analysis to assess the distribution of the lubricant on tablets attendant to the manufacturing processes.

2. Development of non-contact techniques based on computer vision for tracking solvent progression through tablet matrices and quantifying the evolution of the erosion process in pharmaceutical tablets.

3. Development of numerical strategies, augmented and informed by experimental tests, to simulate the drug release profiles for both (diffusion and erosion dominated) systems using a level set based framework.

In the following sections, a summary description of the main contributions in each area is presented.

7.1.1 LIBS analysis

The LIBS technique we employed is extremely sensitive to magnesium and shows great potential in analyzing tablets with even lower ($< 1\%$) concentrations of MgSt. While developing a calibration set for the samples, it became evident that MgSt concentrations of 1.5%(w/w) were already enough to saturate the detector for our given ablation settings. Chemical images of tablets produced from the LIBS signals show the existence of "chunks" of API and/or lubricant at sub surface locations and allow for simple visual examination of material distribution in tablets. As expected, increased strain conditions resulted in tablets with more homogeneously distributed API and lubricant as indicated by the RSD of marker signals for a given tablet. LIBS proved to be useful in determining content distribution of the tablets. However, the average signal values of representative components do not correlate well with the expected content of drug or lubricant in tablets. Thus the technique is not reliably quantitative. The X-ray μCT imaging of LIBS ablated tablets lent insight to the amount of material which was ablated with each shot. The depth to which individual laser pulses removed material was too variable for these samples. While the average depth of an ablation from a single laser pulse was 50 microns, ranging from 60 to 30 microns average for a given shot level, the deviation could be as much as 30 microns. While tablets made from blends which had undergone more total strain produced less variable results, none of the investigated samples produced results consistent enough to qualify the technique as quantitative. It remains unclear whether the material content of an ablation affected the depth achieved in a given pulse. Comparison of signal ratios at each shot produced the most useful information concerning expected tablet performance. Tablets made from blends subjected to higher total strain exhibited lower ratios of the Mg signal to the C_2 signal. We believe this is the result of a greater percentage of the surface area of API and excipient particles being coated with MgSt and this hypothesis is supported by the results of previous research and the model simulations presented herein. The comparison of signal ratios was possible without prior calibration of the signals and indicates microstructural changes in the material induced by high shear blending.

Compactibility of tablets was only nominally changed, though the dissolution performance was markedly changed as a result of shear blending. While there are clear ties between tablet density and dissolution rate, the use of the Presster allowed for the production of samples which are within a tight set of density constraints in a manner consistent with commercial production on a rotary press. In addition, an instrumented commercial rotary press would not self correct for such changes in the blends. Meaning, if a portion of a blend underwent increased shear due to feed frame effects, etc., the changes in material microstructure would not cause enough of a change in compactibility of the material for a commonly instrumented rotary press to detect. This further indicates the importance of post compaction testing of the product. Decreases in drug release rate trend with increases in total strain while shear rate did not produce a consistent effect. We believe the shear mixing causes soluble particles to become coated with hydrophobic MgSt reducing the available surface area of individual particles for dissolution. This claim is supported by the results of the numerical models. As total shear increases, the surface area available for dissolution is reduced through manipulation of a dissolution coefficient. This trend is consistent with the change in MgC_2 signal values collected from the LIBS experiments as indicated in the aforementioned chapter's graphical representations.

7.1.2 Experimental Characterization by Computer Vision

Computer vision analyses of solvent penetration were vital in determining the post swelling dimensions of tablets. Swelling occurred primarily along the axis of compaction. Measurements of solvent penetration rate also indicate that the initial solvent penetration occurs much faster than dissolution of the API. Unfortunately there are no visual indications of a secondary solvent penetration process, though, this is indicated by comparison of the model output with physical dissolution profiles of the tablets with the slowest drug release rates. Total strain had no measureable effect on the solvent penetration rates nor the post penetration swelling of tablets. Analysis of solvent penetration rates of both DCL and Chlorpheniramine blend tablets indicate the molecular sorption model is a better fit to experimental data than the more commonly

used Washburn model. This is mainly due to the initial slope of the Washburn equation which approaches infinity at time equal to zero. In addition, a secondary relaxation or swelling front was noted in the solvent penetration experiments. Further inspection of the relationship between the evolution of the two fronts as well as the overall solvent mass uptake of tablets could improve understanding of the governing mechanisms in each front region.

The expanded two camera computer vision experiments present an excellent proof of concept for capturing surface evolution and more precise information concerning volume changes of eroding tablets during dissolution/disintegration. Our updated setup allowed us to observe the surface geometry of the tablets in a steady flow environment. Fluid shear induced shape changes were not observed in these experiments, unlike previous attempts which indicated shear played a role in localized shape changes. Using this data, we were able to create a model which maintained self similar geometry. Analysis of the physical experiments indicated the propensity of the HPMC matrix to erode along the axis of compression. This is a reasonable observation as previous experiments with the direct compression formulation indicated swelling occurred primarily along the axis of compression.

7.1.3 Numerical Modeling

The results of the compaction and solvent penetration experiments are directly incorporated in the building of the numerical models for the diffusion dominated system. This includes the dimensions before and after swelling which, combined with the true density of materials and mass of a given sample, allows for the calculation of the post swelling porosity and thus the solvent concentration of the tablets. The rate of solvent penetration in the physical experiments allows for the assumption that the model starts out filled with solvent and fully swelled. This greatly reduces the complexity of the simulations. Overall there are 16 parameters to the model considering the dissolution of both API and lactose are incorporated. Once the measurable physical parameters and MSDS data are utilized, there are 2 free parameters for both API and lactose, the dissolution coefficient and solute diffusion coefficient. The solute diffusion coefficients

are set equal and tuned using the trailing data of the physical dissolution experiments so that all tablets have the same solute diffusion coefficients. Thus the model is reduced to 2 free parameters, the particle dissolution coefficients, which are considered to be equal to further reduce the complexity to a one parameter model. The particle dissolution coefficient implicitly considers the percentage of surface area available for dissolution which is the factor expected to be changed between blends. The numerical simulations of the diffusion driven system indicated changes in available surface area of soluble particles can account for the changes observed in the physical dissolution results, at least for the lower shear cases. In the most extreme total strain case, it would appear additional mechanisms govern the release of drug. Secondary changes in the available solvent could account for these differences in the model, but this has not been confirmed as the mechanism of action in the physical tablets.

While the erosion model results diverge from the experimental results at later timepoints, it is possible this is a result of modifications made to tablets to attached to the support rod. These divergences are especially prevalent in the higher shear experiments. However, the experiments in stagnant fluid showed excellent agreement with the numerical model until the very last timepoints. While inclusion of non-uniform shear effects and additional fluid pathways may result in a better model fit, expansion of the experimental data set would be a more useful expenditure of resources.

The models presented here are both able to capture several physical mechanisms. The framework is adaptable to two systems governed by different primary release mechanisms. The main contribution of the framework is the utilization of a level set technique to capturing surface evolution and impose boundary conditions at higher than grid resolutions. This is a truly 3-D model which allows for highly complex model definitions. While both system specific models have a large number of parameters, the experimental and literature data allow us to reduce the number of free parameters to one and two respectively.

7.2 Future Work

Swelling of the excipient matrix has been shown to be an extremely important part of tablet dissolution for certain excipient formulations. Most commonly, the swelling response of HPMC(hydroxy propyl methyl cellulose)[83, 84, 85]. Other excipients, including micro-crystalline cellulose and lactose, can also swell when exposed to solvents. Swelling of the matrix can cause changes in the location of the bulk interface, the rate of solvent uptake, rate of solute diffusion and contribute to internal stresses. We have already begun to perform experiments using video processing to characterize 1-D swelling and solvent penetration parameters. We also plan to measure the swelled volume of individual particles and use simulations to relate this to swelling of the tablet as a whole. Furthermore, the two camera erosion tracking experiments will be continued. A new camera and lens has been purchased, so now both cameras will be computer controlled. This will open the possibility of using advanced methods to synchronize image acquisition as well as perform image processing on the fly. It is our goal to make the camera system mobile so dissolution/disintegration occurring in other apparati can be imaged using this system as well.

In addition to measuring the swelling parameters physically, it will be necessary to make adjustments to the model to include swelling. A cellular automata model which captures the swelling response of HPMC has been recently published[20], which demonstrates a 2-D model of HPMC swelling verified with physical experiments. Incorporating a high resolution 3-D cellular automata model inside the existing grid space would allow for swelling and solvent penetration to be simulated with an increased relevance at an increased resolution. These processes are less computationally expensive than updating the level set function or calculating the ghosting coefficients, thus increasing their resolution would have much less of an effect than increasing overall grid resolution. As previously described we are focusing on a meso-scale model which allows for non homogeneous tablet descriptions, and part of the goal is to resolve the processes involved in tablet dissolution at meaningful resolutions. A mechanistic 1-D model which calculates tablet swelling in response to stress relaxation of individually

swelled particles as a result of solvent penetration using a level set technique has been tested, but scaling to 3-D would cause the model to run orders of magnitude slower than the present framework.

Once swelling effects have been incorporated, we also plan to allow for more methods of model input. Currently, models are built using a simple program which does not have the power of a DEM based approach. It would be extremely useful to directly incorporate results from models of tablet compaction. As another group member is working directly with such models[86], the data produced by these will be the obvious starting point. Once a model can be built using this data, more common formats such as .stl will be considered, as this greatly broadens the range of programs which can then build the initial model. Part of the drive to add recognition of common formats is due to our participation in the Pharmahub project. We are also looking for new ways to extract parameters from physical tablets using techniques such as X-ray tomography and LIBS(Laser Induced Breakdown Spectroscopy).

References

[1] Mannes Minekus. *Development and Validation of a Dynamic Model of the Gastrointestinal Tract*. PhD thesis, Universiteit Utrecht, May 1998.

[2] Kalyana C. Pingali, Kostas Saranteas, Reza Foroughi, and Fernando J. Muzzio. Practical methods for improving flow properties of active pharmaceutical ingredients. *Drug Development and Industrial Pharmacy*, 35(12):1460–1469, 2009. PMID: 19929205.

[3] Franson N.M. Peppas, N.A. The swelling interface number as a criterion for prediction of diffusional solute release mechanisms in swellable polymers. *Journal of Polymer Science: Polymer Physics Edition*, 21(6):983–997, 2003.

[4] Rafael Mendez, Fernando Muzzio, and Carlos Velazquez. Study of the effects of feed frames on powder blend properties during the filling of tablet press dies. *Powder Technology*, 200(3):105 – 116, 2010.

[5] Rafael Mendez, Fernando J. Muzzio, and Carlos Velazquez. Powder hydrophobicity and flow properties: Effect of feed frame design and operating parameters. *AIChE Journal*, 2011.

[6] Rafael Mendez, Francis S. Romanski, and M. Silvina Tomassone. Density behavior of cohesive granular materials. *Powder Technology*, 211(23):189 – 198, 2011.

[7] Kalyana Pingali, Rafael Mendez, Daniel Lewis, Bozena Michniak-Kohn, Alberto Cuitino, and Fernando Muzzio. Evaluation of strain-induced hydrophobicity of pharmaceutical blends and its effect on drug release rate under multiple compression conditions. *Drug Development and Industrial Pharmacy*, 37(4):428–435, 2011.

[8] Kalyana Pingali, Rafael Mendez, Daniel Lewis, Bozena Michniak-Kohn, Alberto Cuitino, and Fernando Muzzio. Mixing order of glidant and lubricant: Influence on powder and tablet properties. *International Journal of Pharmaceutics*, 409(1-2):269 – 277, 2011.

[9] Lobo J.M.S. Costa, P. Modeling and comparison of dissolution profiles. *European Journal of Pharmaceutical Sciences*, 13:123–133, 2001.

[10] NOYES A. A. The rate of solution of solid substances in their own solutions. *J. Am. Chem. Soc.*, 10:930–934, 1897.

[11] E. Brunner. Reaktionsgeschwindigkeit in heterogenen systemen. *Z. Phys. Chem.*, 47:56–102, 1904.

[12] Stuart Feldman Milo Gibaldi. Establishment of sink conditions in dissolution rate determinations. theoretical considerations and application to nondisintegrating dosage forms. *Journal of Pharmaceutical Sciences*, 56(10):1238–1242, 1967.

[13] Ito Y Teramura S Okado J. Kitazawa S, Johno I. Effects of hardness on the disintegration time and the dissolution rate of uncoated caffeine tablets. *J Pharm Pharmacol.*, 27(10):765–70, October 1975.

[14] T. Higuchi. Rate of release of medicaments from ointment bases containing drugs in suspension. *J. Pharm. Sci.*, 50:874–5, 1961.

[15] T. Higuchi. Mechanism of sustained-action medication. theoretical analysis of rate of release of solid drugs dispersed in solid matrices. *J. Pharm. Sci.*, 52:11451149, 1963.

[16] Mayersohn M. Walker G.C. Cobby, J. Influence of shape factors on kinetics of drug release from matrix tablets. *Experimental. J. Pharm. Sci.*, 63:732737, 1974.

[17] Hirotaka Endoh Kozo Ishikawa Kazuhiko Juni Masahiro Nakano Toshinobu Seki, Takeo Kawaguchi. Controlled release of 3prime, 5prime-diester prodrugs of 5-fluoro-2prime-deoxyuridine from poly-2-lactic acid microspheres. *Journal of Pharmaceutical Sciences*, 79(11):985–987, 1990.

[18] Richard W. Korsmeyer, Robert Gurny, Eric Doelker, Pierre Buri, and Nikolaos A. Peppas. Mechanisms of solute release from porous hydrophilic polymers. *International Journal of Pharmaceutics*, 15(1):25 – 35, 1983.

[19] A.R Berens and H.B Hopfenberg. Diffusion and relaxation in glassy polymer powders: 2. separation of diffusion and relaxation parameters. *Polymer*, 19(5):489 – 496, 1978.

[20] Hannu Laaksonen, Jouni Hirvonen, and Timo Laaksonen. Cellular automata model for swelling-controlled drug release. *International Journal of Pharmaceutics*, 380(1-2):25 – 32, 2009.

[21] P.A.C. Gane, C.J. Ridgway, and E. Barcel. Analysis of pore structure enables improved tablet delivery systems. *Powder Technology*, 169(2):77 – 83, 2006.

[22] S.G. Stepanek F. Kimber, J.A. Kazarian. Microstructure-based mathematical modelling and spectroscopic imaging of tablet dissolution. *Computers and Chemical Engineering*, In Press, Corrected Proof, 2010.

[23] Charalambos G. Varelas, David G. Dixon, and Carol A. Steiner. Zero-order release from biphasic polymer hydrogels. *Journal of Controlled Release*, 34(3):185 – 192, 1995.

[24] E. Krausbauer. *Contributions to a Science Based Expert System for Solid Dosage Form Design.* PhD thesis, Universitat Basel, 2007.

[25] J.A. Kimber, S.G. Kazarian, and F. Stepanek. Modelling of pharmaceutical tablet swelling and dissolution using discrete element method. *Chemical Engineering Science*, 69(1):394 – 403, 2012.

[26] J.A. Kimber, S.G. Kazarian, and F. Stepanek. Formulation design space analysis for drug release from swelling polymer tablets. *Powder Technology*, 2012.

[27] Nicklasson M. Johansson ME. Investigation of the film formation of magnesium stearate by applying a flow-through dissolution technique. *J Pharm Pharmacol.*, 38(1):51–4, Jan 1986.

[28] M.S.Hafeez Hussain, Peter York, and Peter Timmins. A study of the formation of magnesium stearate film on sodium chloride using energy-dispersive x-ray analysis. *International Journal of Pharmaceutics*, 42(1-3):89 – 95, 1988.

[29] Z. T. Chowhan and I.-C. Yang. Effect of intergranular versus intragranular cornstarch on tablet friability and in vitro dissolution. *Journal of Pharmaceutical Sciences*, 72(9):983–988, 1983.

[30] K. Zuurman, K. Van der Voort Maarschalk, and G. K. Bolhuis. Effect of magnesium stearate on bonding and porosity expansion of tablets produced from materials with different consolidation properties. *International Journal of Pharmaceutics*, 179(1):107 – 115, 1999.

[31] N.-O. Lindberg, A. Berdal, G. Enstad, E. Seifert, and T. Lundstedt. Investigation of flow properties of powders by means of a uniaxial tester, in relation to direct tablet compression. *Drug Development and Industrial Pharmacy*, 28(1):15–28, 2002.

[32] Z. T. Chowhan. Role of binders in moisture-induced hardness increase in compressed tablets and its effect on in vitro disintegration and dissolution. *Journal of Pharmaceutical Sciences*, 69(1):1–4, 1980.

[33] Z. T. Chowhan and I. C. Yang. Powder flow studies iv. tensile strength and orifice flow rate relationships of binary mixtures. *International Journal of Pharmaceutics*, 14(2-3):231 – 242, 1983.

[34] Moore RD Sheskey PJ, Robb RT. Effects of lubricant level, method of mixing, and duration of mixing on a controlled- release matrix tablet containing hydroxypropyl methylcellulose. *Drug Dev Ind Pharm*, 21:2151–65, 1995.

[35] Kitamori N. Kikuta J. Effect of mixing time on the lubricating properties of magnesium stearate and the final characteristics of the compressed tablet. *Drug Dev Ind Pharm*, 20:343–55, 1994.

[36] G. K. Bolhuis, S. W. De Jong, C. F. Lerk, H. Dettmers, and B. V. Pharbita. The effect of magnesium stearate admixing in different types of laboratory and industrial mixers on tablet crushing strength. *Drug Development and Industrial Pharmacy*, 13(9-11):1547–1567, 1987.

[37] B. van Veen, K. van der Voort Maarschalk, G. K. Bolhuis, and H. W. Frijlink. Predicting mechanical properties of compacts containing two components. *Powder Technology*, 139(2):156 – 164, 2004.

[38] Margaret D. Louey and Peter J. Stewart. Particle interactions involved in aerosol dispersion of ternary interactive mixtures. *Pharmaceutical Research*, 19:1524–1531, 2002. 10.1023/A:1020464801786.

[39] L.J. Cremers, D.A.; Radziemski. *Handbook of Laser-Induced Breakdown Spectroscopy*. Wiley: New York, 2006.

[40] V.; Schechter I. Misiolek, A.W.; Palleschi. *Laser Induced Breakdown Spectroscopy: Fundamental and Applications*. Cambridge University Press: Cambridge, 2006.

[41] L. St-Onge, E. Kwong, M. Sabsabi, and E. B. Vadas. Quantitative analysis of pharmaceutical products by laser-induced breakdown spectroscopy. *Spectrochimica Acta Part B: Atomic Spectroscopy*, 57(7):1131 – 1140, 2002.

[42] Jennifer Wang, Hong Wen, and Divyakant Desai. Lubrication in tablet formulations. *European Journal of Pharmaceutics and Biopharmaceutics*, 75(1):1 – 15, 2010.

[43] Gabriel Gustinelli Arantes de Carvalho, Lidiane Cristina Nunes, Paulino Florencio de Souza, Francisco Jose Krug, Thaisa Correia Alegre, and Dario Santos Jr. Evaluation of laser induced breakdown spectrometry for the determination of macro and micronutrients in pharmaceutical tablets. *J. Anal. At. Spectrom.*, 25:803–809, 2010.

[44] M. Abdelhamid, S. Grassini, E. Angelini, G.M. Ingo, and M.A. Harith. Depth profiling of coated metallic artifacts adopting laser-induced breakdown spectrometry. *Spectrochimica Acta Part B: Atomic Spectroscopy*, 65(8):695 – 701, 2010. A Selection of Papers Presented at the 5th Euro-Mediterranean Symposium on Laser Induced Breakdown Spectroscopy (EMSLIBS 2009).

[45] S. Amoruso, M. Armenante, V. Berardi, R. Bruzzese, and N. Spinelli. Absorption and saturation mechanisms in aluminium laser ablated plasmas. *Applied Physics A: Materials Science and Processing*, 65:265–271, 1997. 10.1007/s003390050577.

[46] Jess Anzano, Beatriz Bonilla, Beatriz Montull-Ibor, and Justiniano Casas-Gonzlez. Rapid characterization of analgesic pills by laser-induced breakdown spectroscopy (libs). *Medicinal Chemistry Research*, 18:656–664, 2009. 10.1007/s00044-008-9157-5.

[47] C. CHALEARD, P. MAUCHIEN, N. ANDRE, J. UEBBING, J. L. LACOUR, and C. GEERTSEN. Correction of matrix effects in quantitative elemental analysis with laser ablation optical emission spectrometry. *J. Anal. At. Spectrom.*, 12:183–188, 1997.

[48] Louis St-Onge. A mathematical framework for modeling the compositional depth profiles obtained by pulsed laser ablation. *J. Anal. At. Spectrom.*, 17:1083–1089, 2002.

[49] E. Tognoni, G. Cristoforetti, S. Legnaioli, and V. Palleschi. Calibration-free laser-induced breakdown spectroscopy: State of the art. *Spectrochimica Acta Part B: Atomic Spectroscopy*, 65(1):1 – 14, 2010.

[50] Gina Massimo, Pier Luigi Catellani, Patrizia Santi, Ruggero Bettini, Gianluigi Vaona, Alessandro Bonfanti, Loretta Maggi, and Paolo Colombo. Disintegration propensity of tablets evaluated by means of disintegrating force kinetics. *Pharmaceutical Development and Technology*, 5(2):163–169, 2000.

[51] Turner Alfrey, E. F. Gurnee, and W. G. Lloyd. Diffusion in glassy polymers. *Journal of Polymer Science Part C: Polymer Symposia*, 12(1):249–261, 1966.

[52] J. Crank. *The mathematics of diffusion.* Oxford: Clarendon Press, 2nd edition, 1975.

[53] P. J. McDonald, J. Godward, R. Sackin, and R. P. Sear. Surface flux limited diffusion of solvent into polymer. *Macromolecules*, 34(4):1048–1057, 2001.

[54] D. Vesely. Diffusion of liquids in polymers. *International Materials Reviews*, 53(5):299–315, 2008.

[55] R. Konrad, A. Christ, G. Zessin, and U. Cobet. The use of ultrasound and penetrometer to characterize the advancement of swelling and eroding fronts in hpmc matrices. *International Journal of Pharmaceutics*, 163(12):123 – 131, 1998.

[56] R. Luginbuhl and H. Leuenberger. Use of percolation theory to interpret water uptake, disintegration time and intrinsic dissolution rate of tablets consisting of binary mixtures. *Pharmaceutica Acta Helvetiae*, 69(3):127 – 134, 1994.

[57] Edward W. Washburn. The dynamics of capillary flow. *Phys. Rev.*, 17:273–283, Mar 1921.

[58] P Morrissey and D Vesely. Accurate measurement of diffusion rates of small molecules through polymers. *Polymer*, 41(5):1865 – 1872, 2000.

[59] David A. Bond and Paul A. Smith. Modeling the transport of low-molecular-weight penetrants within polymer matrix composites. *Applied Mechanics Reviews*, 59(5):249–268, 2006.

[60] N.L. Thomas and A.H. Windle. A deformation model for case ii diffusion. *Polymer*, 21(6):613 – 619, 1980.

[61] J. C. Wu and Nikolaos A. Peppas. Modeling of penetrant diffusion in glassy polymers with an integral sorption deborah number. *Journal of Polymer Science Part B: Polymer Physics*, 31(11):1503–1518, 1993.

[62] J. C. Wu and Nikolaos A. Peppas. Numerical simulation of anomalous penetrant diffusion in polymers. *Journal of Applied Polymer Science*, 49(10):1845–1856, 1993.

[63] D. Vesely. The rate of solvent diffusion in amorphous polymers. *Macromolecular Symposia*, 138(1):215–223, 1999.

[64] D. Vesely. Molecular sorption mechanism of solvent diffusion in polymers. *Polymer*, 42(9):4417 – 4422, 2001.

[65] Jennifer L. Baxter, Joseph Kukura, and Fernando J. Muzzio. Hydrodynamics-induced variability in the usp apparatus ii dissolution test. *International Journal of Pharmaceutics*, 292(1-2):17 – 28, 2005.

[66] J. Kukura, J. L. Baxter, and F. J. Muzzio. Shear distribution and variability in the usp apparatus 2 under turbulent conditions. *International Journal of Pharmaceutics*, 279(1-2):9 – 17, 2004.

[67] Bradski G. *The OpenCV library.* Dr. Dobbs J Soft Tools, Nov 2000. Available from: http://drdobbs.com/open-source/184404319.

[68] Daniel Braido. Modeling and simulation of release profiles due to coupled dissolution and erosion mechanisms. Master's thesis, Rutgers University, Dept. of MAE, 2010.

[69] J.A. Osher, Sethian. *Level Set Methods and Fast Marching Methods: Evolving Interfaces in Computational Geometry, Fluid Mechanics, Computer Vision, and Materials Science*. Cambridge University Press, 1996.

[70] Kinjal Dhruva. Modeling dynamic void growth and coalescence by plasticity and diffusion using a level set approach. Master's thesis, Rutgers University, Dept. of MAE, 2004.

[71] E. Javierre, C. Vuik, F.J. Vermolen, and A. Segal. A level set method for three dimensional vector stefan problems: Dissolution of stoichiometric particles in multicomponent alloys. *Journal of Computational Physics*, 224(1):222 – 240, 2007. Special Issue Dedicated to Professor Piet Wesseling on the occasion of his retirement from Delft University of Technology.

[72] Peppas N.A. Siepmann, J. Hydrophilic matrices for controlled drug delivery: An improved mathematical model to predict the resulting drug release kinetics (the sequential layer model). *Pharmaceutical Research*, 17:1290–1298, 2000.

[73] Yanxing Wang, Bertil Abrahamsson, Lennart Lindfors, and James G. Brasseur. Comparison and analysis of theoretical models for diffusion-controlled dissolution. *Molecular Pharmaceutics*, 0(ja):null, 2012.

[74] Peppas N.A. Ritger, P.L. A simple equation for description of solute release i. fickian and non-fickian release from non-swellable devices in the form of slabs, spheres, cylinders or discs. *Journal of Controlled Release*, 5(1):23–35, 1986.

[75] Kalyana Pingali, Rafael Mendez, Daniel Lewis, Bozena Michniak-Kohn, Alberto Cuitio, and Fernando Muzzio. Evaluation of strain-induced hydrophobicity of pharmaceutical blends and its effect on drug release rate under multiple compression conditions. *Drug Development and Industrial Pharmacy*, 0(0):1–9, 0.

[76] Kwong E Sabsabi M Vadas EB. St-Onge L, Archambault JF. Rapid quantitative analysis of magnesium stearate in tablets using laser-induced breakdown spectroscopy. *J Pharm Sci.*, 8(2):272–88, 2005.

[77] A. Ciucci, M. Corsi, V. Palleschi, S. Rastelli, A. Salvetti, and E. Tognoni. New procedure for quantitative elemental analysis by laser-induced plasma spectroscopy. *Appl. Spectrosc.*, 53(8):960–964, Aug 1999.

[78] Nikita B. Zorov, Alexander A. Gorbatenko, Timur A. Labutin, and Andrey M. Popov. A review of normalization techniques in analytical atomic spectrometry with laser sampling: From single to multivariate correction. *Spectrochimica Acta Part B: Atomic Spectroscopy*, 65(8):642 – 657, 2010. A Selection of Papers Presented at the 5th Euro-Mediterranean Symposium on Laser Induced Breakdown Spectroscopy (EMSLIBS 2009).

[79] Influence of shear intensity and total shear on properties of blends and tablets of lactose and cellulose lubricated with magnesium stearate. *International Journal of Pharmaceutics*, 336(2):284 – 291, 2007.

[80] Changquan (Calvin) Sun. True density of microcrystalline cellulose. *Journal of Pharmaceutical Sciences*, 94(10):2132–2134, 2005.

[81] Mazen L. Hamad, Abhay Gupta, Rakhi B. Shah, Robbe C. Lyon, Vilayat A. Sayeed, and Mansoor A. Khan. Functionality of magnesium stearate derived from bovine and vegetable sources: Dry granulated tablets. *Journal of Pharmaceutical Sciences*, 97(12):5328–5340, 2008.

[82] Bertil Abrahamsson, Anupam Pal, Marie Sjberg, Maria Carlsson, Emma Laurell, and James G. Brasseur. A novel in-vitro and numerical analysis of shear-induced drug release from extended-release tablets in the fed stomach. *Pharmaceutical Research*, 22:1215–1226, 2005. 10.1007/s11095-005-5272-x.

[83] Philip L. Ritger and Nikolaos A. Peppas. A simple equation for description of solute release ii. fickian and anomalous release from swellable devices. *Journal of Controlled Release*, 5(1):37 – 42, 1987.

[84] Nikolaos A. Peppas and Jennifer J. Sahlin. A simple equation for the description of solute release. iii. coupling of diffusion and relaxation. *International Journal of Pharmaceutics*, 57(2):169 – 172, 1989.

[85] Kosmas Kosmidis, Eleni Rinaki, Panos Argyrakis, and Panos Macheras. Analysis of case ii drug transport with radial and axial release from cylinders. *International Journal of Pharmaceutics*, 254(2):183 – 188, 2003.

[86] Athanas Koynov. Correlation between excipient characteristics and product properties through numerical simulations of tablet compaction. AIChE, November 2008.

Vita

Daniel Braido

2004 Graduated from Carnegie Mellon University

2004-2010 **Rutgers University**
Masters Mechanical Engineering.

2011-2012 **Rutgers University**
PhD. Chemical and Biochemical Engineering.

2005 - 2012 Graduate Assistant.

Safety

Appropriate safety measures were taken whilst performing all physical experiments. Proper PPE(personal protective equipment) was worn at all times in the lab. This includes lab coat, nitrile gloves, safety glasses and where necessary due to powder handling, a half face respirator. Furthermore, all samples were stored in properly labeled containers and waste materials were disposed of in designated pharmaceutical waste receptacles.